Arctic Freshwater Export Drives Reduction of the Subpolar North Atlantic Carbon Sink (1990-2100)

by

Sean M. Ridge

A thesis submitted in partial fulfillment of the requirements for the degree of

Master's of Science

(Atmospheric and Oceanic Sciences)

at the

University of Wisconsin – Madison

2017

Contents

Acknowledgements

Thank you, Emily, for the support you have steadily provided me. I admire your work ethic and persistence, and you have cultivated my personal growth in those areas. What you have done for me, our relationship, and our home leaves me feeling immense gratitude to have you as my wife.

And thank you, Galen, for your mentorship. Your expert guidance in my research has contributed so much intellectually and also my timely progress. Also, you have provided multiple opportunities for professional development that have been a great benefit to me. Thank you for what you have provided so far, and I deeply appreciate the opportunities you have provided both me and my wife by offering me the ability to continue as your student at Columbia University.

Abstract

The subpolar North Atlantic covers only 2.3% of the global ocean area, but plays an important role in the global carbon cycle. As the most intense carbon sink per unit area, the subpolar North Atlantic accounts for 12% of the 1.7 Pg C yr^{-1} of global ocean carbon uptake (Schuster et al. 2013, Takahashi et al. 2009) We consider the future evolution of this critical carbon sink using the physical and biogeochemistry output from the CESM Large Ensemble Community Project (LENS). We define "high intensity air-sea anthropogenic carbon (C_{ant}) flux regions" as those where the strength of the flux is >80^{th} percentile. For the historical era in CESM-LENS, high flux intensity regions constitute a disproportionate share of the total ocean carbon uptake, responsible for 40% of the global anthropogenic carbon uptake while comprising only 20% of total ocean area. Over 1990-2100, there is a shift of high intensity flux away from the North Atlantic and to the Southern Ocean. The subpolar North Atlantic is the only high intensity uptake region with projected reduction of anthropogenic carbon uptake. This sharp reduction in North Atlantic carbon uptake is driven by amplification of the Arctic hydrological cycle and resulting changes in a net flux of surface freshwater from the Arctic to the Atlantic. The high DIC and low alkalinity of Arctic surface freshwater reduces the sea-air pCO_2 difference (ΔpCO_2), and thus the air-sea carbon flux. Using modeled fields of salinity and ΔpCO_2, we compare the results from the CESM-LENS to other global climate models included in the Coupled Model Intercomparison Project Phase 5 (CMIP5). All CMIP5 models display similar salinity trends of the subpolar gyre. These effects of freshwater on pCO_2 are an example of an intense climate-carbon cycle feedback mechanism projected to occur in the Arctic-North Atlantic.

1. Introduction

The ocean has consistently provided the critical service of carbon uptake. Over the industrial era, the ocean has been a carbon sink and is responsible for the uptake of 40% of anthropogenic carbon emissions over this time period (Sabine et al. 2004, Khatiwala et al. 2009, Ciais et al. 2013). It is unlikely that this service will continue invariably into the future, as the various effects of a warming climate are expected to project onto the carbon cycle, via both physical and biogeochemical mechanisms. Climate projections from earth system models are in agreement that the response of the ocean to warming in high emission scenarios will result in a decrease in oceanic carbon uptake relative to the increase in carbon oceanic carbon uptake due to increasing carbon emissions in a high emission scenario (Friedlingstein et al. 2003, Ciais et al. 2013, Randerson et al. 2015). Increases to the atmospheric concentration of CO_2 will act to drive more carbon into the ocean, while climate change will act in opposition and decrease global carbon uptake potential, which is primarily due to the stratification of the upper ocean. How climate change interacts with the carbon cycle regionally deserves closer inspection because the dominant mechanisms driving carbon uptake vary region to region. Multiple studies suggest that carbon uptake in the North Atlantic may have a uniquely strong negative response to climate change (Randerson et al. 2015, McKinley et al. 2016).

The North Atlantic is a region of intense uptake of atmospheric CO_2, representing only 13% of the surface area of the ocean, but responsible for a third of the global ocean CO_2 uptake. The subpolar front separates two biogeochemically distinct sub regions of the

North Atlantic: the high latitude subpolar, containing the subpolar gyre and adjacent Nordic seas, and the subtropical North Atlantic. Despite the small area relative to other regions like the Southern Ocean, the subpolar region (49˚ N – 76˚ N) has been estimated to account for 12% of the 1.7 $PgCyr^{-1}$ of global ocean carbon uptake, all while covering only 2.3% of the global ocean area (Gruber et al. 2009; Schuster et al. 2013). Because of unique carbon uptake processes, the subpolar region has twice the flux intensity per unit area (2.0 $molCm^{-2}$) as compared to the subtropical North Atlantic (1.0 $molCm^{-2}$) (Takahashi et al. 2009). The high flux intensity relative to other regions is due to rapid cooling of waters flowing north from the subtropics, which increases CO_2 solubility. Strong wind stress and deep convection intermittently force mixed layer depth (MLD) down below 2km in this region, a process that promotes subduction to the deep ocean of surface waters carrying a high anthropogenic carbon load (Sabine et al. 2004, Khatiwala et al. 2013, Devries 2014). This mixing also replenishes nutrients to the euphotic zone each winter and allows for the seasonal drawdown of surface pCO_2 by the intense springtime phytoplankton blooms in this region that further enhances net carbon uptake (Takahashi et al. 2009, Schuster et al. 2013). Warming, as well as reductions in MLD and reduced primary productivity would all result in reduced uptake of CO_2.

Deep convection, driving deep MLD in this region, requires strong negative surface buoyancy fluxes, provided by potent surface cooling. This process has large interannual and multidecadal variability, where in recent decades the Labrador, Irminger, and Greenland seas have gone many years without a major event (Marshall and Schott 1999, Lazier et al. 2002, Våge et al. 2008). Changes in deep convection have been linked to slowing of the

circulation in the subpolar region (Häkkinen and Rhines 2004). Excluding the Mediterranean, semi-regular deep convection only occurs in the seas of the high latitude North Atlantic (Marshall and Schott 1999, de Lavergne et al. 2014), and convection could have halted during past climates as indicated by observations (Thornalley et al. 2011). Deep water formation, supported by deep convection, is believed to drive the lower segment of the Atlantic Meridional Overturning Circulation (AMOC). The lower limb helps transport carbon rich water out of the subpolar gyre, and in years where the AMOC is weakened, atmospheric carbon uptake in the subpolar North Atlantic may be reduced (Pérez et al. 2013). Not only are these changes important to the regional climate of North America and Europe, but a slowdown in the AMOC could also reduce the amount of carbon stored in the deep ocean.

Model and observational studies suggest that as Earth's climate warms, the Nordic seas and the subpolar gyre will be subjected to increases in freshwater from precipitation, increased Arctic freshwater export, and increased runoff from Greenland. Increased freshwater supply may slow down AMOC (Stouffer et al. 2006; Jahn et al. 2010a; Swingedouw et al. 2013). The Arctic Ocean has a low salinity due to receiving a relatively high amount of river output – accepting 11% of the global river discharge into only 1% of the global ocean volume (Gleick 2000, Dai and Trenberth 2002). The North Atlantic receives freshwater from the Arctic through the export of both liquid freshwater and sea ice (Aagard and Carmack 1989, Carmack 2000, Karcher et al. 2005, Dickson et al. 2007, Polyakov et al. 2008). The low density of freshwater confines much of the freshwater export to the mixed

layer, which also maximizes the stratification effect it could have when exported to regions of subpolar North Atlantic deep mixing.

The first order controls on the export of liquid freshwater and sea ice from the Arctic basin into the North Atlantic are the general atmospheric circulation of the Arctic and the freshwater content of the Arctic (Haine et al 2015). Arctic amplification, the high degree of warming the Arctic has experienced relative to the rest of the globe (Serreze and Barry 2011), could act to alter these controlling mechanisms and increase freshwater export from the Arctic, into the North Atlantic. Model studies indicate that a more intense Arctic hydrological cycle is occurring in association with this amplification (Rawlins et al. 2010, Vavrus et al. 2012, Koenigk et al. 2012). These feedbacks could result in increased freshwater export through changing large scale atmospheric circulation and freshening of Arctic waters (Holland et al. 2007, Morison et al. 2012, Vavrus et al. 2012, Koenigk et al. 2012).

Multi-year declines in alkalinity have been observed in the Arctic's Canada Basin and attributed to increased runoff, decreased sea-ice volume, and increased precipitation (Yamamoto-Kawai et al. 2009). If these freshwater sources have substantially lower alkalinity than seawater, these fluxes of freshwater from the Arctic will directly reduce CO_2 solubility by reducing the buffering capacity of seawater. Freshwater fluxes can also indirectly impact the carbon cycle, by altering circulation, and reducing vertical mixing that supplies nutrients and thus limiting biological drawdown of carbon in the surface ocean. With this in mind, we ask: *How will increased Arctic freshwater export to the North Atlantic impact the ocean carbon sink through 2100?*

Given the lack of available biogeochemical data, we evaluate our hypothesis with biogeochemistry output from the Community Earth System Model - Large Ensemble (CESM-LENS) experiment (Kay et al. 2015). Our focus is on the physical and biogeochemical drivers of air-sea exchange, specifically changes to surface ocean pCO_2, which is proportional to the air-sea flux of carbon. Many observations of surface ocean pCO_2 come from volunteer observing ships (Takahashi et al. 2009, Bakker et al. 2016). The lack of ship traffic in the subpolar North Atlantic and Arctic contributes to sparse in-situ observations in these regions. Model simulations, validated with the few observations that exist, offer a platform with which mechanistic relationships can be studied. Model-based projections can indicate the likely future impacts on the ocean carbon cycle of anthropogenic climate change. It is also important to consider the natural variability when studying climate, especially in a region such as the subpolar North Atlantic and Arctic which exhibits a high degree of variability (Swart et al. 2015, McKinley et al. 2016). The CESM-LENS allows for us to examine climate variability, the forced response to climate change, and understand future impacts of climate change on the carbon cycle.

2. Methods

2.1 Model

The National Center for Atmospheric Research (NCAR) CESM Large Ensemble Community Project (CESM-LENS) is a publically available initial condition ensemble simulating climate variability and climate response over the period 1920-2100 (Kay et al. 2015). The CESM is a state of the art earth system model with components simulating the

atmosphere, ocean, land surface, and sea ice. For the CEMS-LENS experiment, the ocean model was spun up for 402 years as part of the control integration; run with constant preindustrial forcing and with tracers initialized from modern day observations. Distribution of biogeochemical tracers came from a separate simulation integrated for 600 years. Once the deep ocean was considered to be in equilibrium, ensemble member 1 was then integrated with historical forcing over the period 1850-2005 and Representative Concentration Pathway 8.5 (RCP 8.5) forcing was used for the integration period 2006-2100. All additional ensemble members are initialized from ensemble member 1 on January 1, 1920 with round-off level differences in the atmospheric temperature field. Because of the short memory and chaotic nature of the atmosphere, after a month of integration, the ensemble diverges and each ensemble member has a unique trajectory.

Utilizing a large ensemble rather than a single model allows the experimenter to explicitly separate the forced response from natural interannual variability (Deser et al. 2012b). We leverage this experimental design to determine whether the carbon cycle response we see in the climate simulation can be attributed to climate change with 95% certainty (the forced climate response). With a large ensemble we are able to determine the forced trend over more of the simulation compared to the smaller ensembles common in CMIP5. In these smaller ensembles and single realizations, natural climate variability masks the forced trend when the trend is calculated for short lengths of time (Deser et al. 2012b). This experimental design also permits us to answer questions concerning whether anthropogenically forced changes will alter carbon cycle and climate variability.

The focus of this study is the period from 1990-2100. The study period allows for comparison to observations of freshwater fluxes for validation purposes, and also provides insight into how the carbon cycle will respond to anthropogenic forcing. The model accurately simulates annual carbon flux magnitude and variability (McKinley et al. 2016). More general discussion of ocean biogeochemistry simulation performance can be found in Long et al. (2013) Moore et al. (2013) and Lindsay et al. (2014). Arctic sea ice properties, variability, and trends are considered to be well simulated in the model (Jahn et al. 2012, Barnhart et al. 2016).

2.2 Study Region

The study region is defined by the region south of the major freshwater gateways (Aagard and Carmack 1989) at the northern limits and the southern terminus is at 49˚N (Figure 1). We will show in the following that the proximity to the primary Arctic freshwater gateways, and distribution of Arctic freshwater in the North Atlantic determines the modeled pattern of increased oceanic pCO_2 and positive trends in ΔpCO_2. Analysis using a study region defined by biomes, such as those suggested by Fay and McKinley (2014) or Longhurst (2007), does not significantly differ from the analysis that uses the latitudes selected.

2.3 Anthropogenic Carbon

Air-sea carbon fluxes (Φ_{as}) can be separated into fluxes of natural carbon (Φ_{nat}) and anthropogenic carbon (Φ_{ant}):

$$\Phi_{as} = \Phi_{nat} + \Phi_{ant}$$

Φ_{nat} is the carbon fluxed between the ocean and atmosphere if the surface ocean was experiencing a partial pressure of atmospheric CO_2 (pCO_2^{atm}) that has remained at preindustrial values.Φ_{ant} is the remainder of the carbon that is fluxed across the ocean-atmosphere interface, which is then only the response to increasing pCO_2^{atm}.

We calculate Φ_{ant} by residual from the standard output of Φ_{as} and Φ_{nat} and their ensemble mean values from the CESM-LENS. To calculate Φ_{nat} the biogeochemical component of each ensemble member is forced with a preindustrial value pCO_2^{atm} of 280 ppm. Φ_{as} is calculated by forcing the biogeochemical component of the model with RCP8.5 pCO_2^{atm} values. The CESM biogeochemistry model allows for the calculation of Φ_{nat} concurrently with the calculation of the total air-sea flux of carbon Φ_{as} without the need for complimentary simulations with preindustrial pCO_2^{atm} forcing for each ensemble member. We take the ensemble average of Φ_{nat} and Φ_{as} and then difference to arrive the ensemble mean value for Φ_{ant}.

2.4 Transport Calculations

We calculate the net freshwater flux to the North Atlantic from the Arctic as:

For liquid freshwater:

$$FW_{liquid} = V_T \frac{S_0 - S_{sw}}{S_0}$$

For solid freshwater:

$$FW_{solid} = V_{T,i} \frac{S_0 - S_i}{S_0} \frac{\rho_i}{\rho_{sw}}$$

Where S_0 is the reference salinity, V_T and $V_{T,i}$ are volume transports for sea water and sea ice respectively. S_{sw} and S_i are the salinities of seawater and sea ice, and ρ_i and ρ_{sw} are the densities of ice and sea water, respectively. We use an S_0 of 34.8, suggested by (Aagard and Carmack 1989) as the mean Arctic salinity. This is an accepted value previously used by Karcher et al. 2005, Holland et al. 2007, Dickson et al. 2007, Polyakov et al. 2008, Jahn et al. 2010, and others.

Liquid freshwater transport is calculated normal to a path intersecting with grid cells (orange dotted line in figure 2). This method allows for better comparison to observations because the transects are a better approximation of oceanographic sections than model transports. Comparing our method to a calculation emulating the model transport equations yields only small differences in the transport analysis. Volume transports for sea ice are calculated from mass transports along open north and east grid cell faces, a standard model output from the sea ice model of CESM, the Los Alamos Sea Ice Model. Volume transports for sea ice are calculated with a different method for ease of analysis and using two different methods has no significant impact on results.

2.5 Linear pCO_2 decomposition

Changes in surface ocean pCO_2 are driven by changes to the biogeochemical properties of ocean surface water. The effect of biogeochemical element cycling on pCO_2^{ocn} is independent from the physical effects of dilution/concentration of biogeochemical properties (freshening effect) so a method to analyze their individual contributions separately would be best suited for our purposes. The current method for calculating pCO_2^{ocn} does not allow for a simple separation of the freshwater effects from

biogeochemical effects so instead we use a Taylor series approximation of pCO_2^{ocn}. This method has been widely used in the field of ocean biogeochemistry to identify the dominant drivers of decadal changes in pCO_2^{ocn} (Keeling et al. 2004, Sarmiento and Gruber, 2006, Lovenduski et al. 2007, Doney et al. 2009, Rödenbeck et al. 2013). The approximation is derived beginning with a linearization of time varying DIC and Alkalinity:

$$DIC(t) = \frac{S(t)}{S_0} sDIC(t), \qquad Alk(t) = \frac{S(t)}{S_0} sAlk(t) \qquad eq.1$$

$$sDIC = \frac{S_0}{S(t)} DIC(t), \qquad sAlk(t) = \frac{S_0}{S(t)} Alk(t) \qquad eq.2$$

Salinity normalization of a biogeochemical variable can be done as shown in equation 2, for DIC and alkalinity. S_0 is a reference salinity (global average, and considered constant) and S(t) is the coincident time-varying salinity. The lowercase *s* prefix is used in the ocean biogeochemistry literature to denote that a variable has been salinity normalized to limit confusion when dealing with salinity normalized and raw values biogeochemical variables.

Linearized equation 2:

$$DIC' = \underbrace{\frac{S'\overline{sDIC}}{S_0}}_{\substack{concentration \\ change}} + \underbrace{\frac{sDIC'\bar{S}}{S_0}}_{\substack{biogeochemical \\ change}}, Alk' = \underbrace{\frac{S'\overline{sAlk}}{S_0}}_{\substack{concentration \\ change}} + \underbrace{\frac{sAlk'\bar{S}}{S_0}}_{\substack{biogeochemical \\ change}} \qquad eq.3$$

$note: X' = \Delta X \quad \overline{X} = intial\ state$

This linearization of changes to DIC and Alkalinity (ΔDIC and ΔAlk) allows for the separation of the total change into changes due to changes in concentration (freshening) and changes

due to biogeochemical changes. We then substitute this equation 3 into our simplified Taylor series expansion of the pCO_2 equation:

$$\Delta pCO_2^{ocn} \approx \frac{\partial pCO_2^{ocn}}{\partial DIC}\Delta DIC + \frac{\partial pCO_2^{ocn}}{\partial Alk}\Delta Alk + \frac{\partial pCO_2^{ocn}}{\partial T}\Delta T \qquad eq.4$$

$$\frac{\partial pCO_2^{ocn}}{\partial DIC}\Delta DIC = \frac{\overline{sDIC}}{S_0}\frac{\partial pCO_2^{ocn}}{\partial DIC}\Delta S + \frac{\overline{S}}{S_0}\frac{\partial pCO_2^{ocn}}{\partial DIC}\Delta sDIC \qquad eq.5$$

$$\frac{\partial pCO_2^{ocn}}{\partial Alk}\Delta Alk = \frac{\overline{sAlk}}{S_0}\frac{\partial pCO_2^{ocn}}{\partial Alk}\Delta S + \frac{\overline{S}}{S_0}\frac{\partial pCO_2^{ocn}}{\partial Alk}\Delta sAlk \qquad eq.6$$

The last term on the right hand side (RHS) of equation 4 is the change in pCO_2^{ocn} due to increases in sea surface temperature (SST). Rising SST results in reduced pCO_2 solubility. The first terms on the RHS on equations 5 and 6, and an added solubility/dissociation term ($\frac{\partial pCO_2^{ocn}}{\partial S}\Delta S$, relatively small) which represents the change in pCO_2 due to changing solubility/dissociation constants (Appendix A), can be combined as:

$$\frac{\partial pCO_2^{ocn}}{\partial FW}\Delta FW = \frac{\overline{sDIC}}{S_0}\frac{\partial pCO_2^{ocn}}{\partial DIC}\Delta S + \frac{\overline{sAlk}}{S_0}\frac{\partial pCO_2^{ocn}}{\partial Alk}\Delta S + \frac{\partial pCO_2^{ocn}}{\partial S}\Delta S \qquad eq.7$$

The full equation is then as follows:

$$\Delta pCO_2^{ocn} \approx \underbrace{\frac{\overline{S}}{S_0}\frac{\partial pCO_2^{ocn}}{\partial Alk}\Delta sAlk}_{pCO_2-sAlk} + \underbrace{\frac{\overline{S}}{S_0}\frac{\partial pCO_2^{ocn}}{\partial DIC}\Delta sDIC}_{pCO_2-sDIC} + \underbrace{\frac{\partial pCO_2^{ocn}}{\partial FW}\Delta FW}_{pCO_2-FW} \qquad eq.8$$

In this study we calculate the partial derivatives of pCO_2^{ocn} by inputting small perturbations of the inputs into the full system of equations used to determine pCO_2^{ocn}. Previous studies used approximations of buffer factors to determine the partial derivatives but that is a less direct method for calculating the sensitivities (partial derivatives) compared to the method used here (Lovenduski et al. 2007, Doney et al. 2009).

2.6 Linearized ΔpCO_2^{ocn} Analysis

Linear analysis requires perturbations to be sufficiently small in order for the linear approximation to have the necessary precision. To satisfy the condition of sufficiently small perturbations, the linear pCO_2^{ocn} analysis is incremented in 20 year intervals and the analysis is applied to each ensemble member individually. To further smooth interannual variability we not only take the ensemble average, but we also average changes with 5 different start years/end years (for example, average of 1990-2009,1991-2010,1992-2011,1993-2012,1994-2013). The result is an approximation of the 20 year change in pCO_2 by each component individually (pCO_2 – DIC, pCO_2 – Alk, pCO_2 – FW). The 20-year differences for each component are summed to represent integrated change attributed to the respective component over the analysis period (1992-2092).

2.7 CMIP5 Climate Simulation Selection

In order to evaluate the robustness of our results, we compared the CESM-LENS to a suite of transient climate simulations from CMIP5 models. These simulations are publically available and hosted online by Earth System Grid Federation (ESGF). Linear trends were calculated over the period of RCP 8.5 forcing (2006-2100) for the models listed in table 1. Model consensus can be exaggerated when assuming all available model simulations are structurally independent, when some simulations are from models with nearly identical components. We exclude simulations from our study due to insufficient simulation of large scale regions of carbon sources/sinks, those from variants of models that are already represented but lack a carbon cycle/ecosystem model, or because the simulation was a low resolution variant (table 2). The INM-CM4 simulation is the only simulation excluded due to

simulation accuracy. It fails to reproduce multiple large scale features of the carbon cycle, for example: the equatorial regions are modeled as a carbon sink, high latitude Northern Hemisphere is modeled as a source (Anav et al 2013). Exclusion of low resolution model variants and variants that lack carbon cycle simulation is done to reduce the exaggeration of the model diversity, but does not entirely eliminate this because some of these coupled models share ocean models and or other earth system component models.

3. Results

3.1 Global Distribution of High Intensity Carbon Uptake

The most vigorous ocean carbon uptake occurs in high latitude ocean regions as shown by observational estimates of carbon flux density (Takahashi et al. 2009, Gruber et al. 2009, Landschützer et al. 2014). These fluxes are well depicted in the CESM-LENS over the period 1982-2011 (McKinley et al. 2016). Maxima in carbon uptake are located in the Southern Ocean and the North Atlantic, whereas the equatorial regions are sources of carbon to the atmosphere (Figure 3a). This is generally consistent with observations for the observed period, and further discussion of CESM carbon cycle model performance can found in Long et al. (2013). Given that our model performs well in comparison to observations, we have confidence in our use of projections from this model to understand how the carbon cycle responds to climate change.

Decadal changes in carbon uptake (Figure 3b-l) reveal a strong forced carbon cycle response in the subpolar North Atlantic. The CESM-LENS projects that decreases in integrated air-sea carbon flux (Φ_{as}) will expand in the region, with the negative signal

initially appearing south of the Labrador Sea, and propagating eastward across the subpolar gyre. The broad region of negative carbon uptake change is greater than 0.5 mol C yr^{-1} and significant at the 95% confidence interval in every period starting with 2000-2009 (Figure 3c) in the decadal differences shown (Figure 3b-l). By 2100, areas within the North Atlantic that were initially rapidly growing sinks of carbon become rapidly declining sinks as this signal expands throughout the region. The response in the region is unique in that the region transitions from strong growth in carbon uptake, to strong decline in uptake and this region is also unrivaled in the open ocean with respect to the strength decline in uptake.

The patterns in Φ_{as} contain changes to both the natural carbon cycle, and the anthropogenic carbon cycle. Changes to the air-sea flux of natural carbon, Φ_{nat}, carbon that has been stored within the ocean for thousands of years, are only driven by changes to circulation and biology. Changes to the air-sea flux of anthropogenic carbon, Φ_{ant}, is only the carbon accumulation due to increasing atmospheric CO_2. Linear trends in Φ_{ant} (Figure 4a) illustrate whether the ocean will be able to keep pace with increases in pCO_2^{atm} and thus continue to be a sink of anthropogenic atmospheric carbon. The trend is clearly nonlinear, but the spatial pattern of the change is similar to the linear trend through 2070 so it is useful in displaying the spatial pattern in a more compact manner. There is a broad region of negative trends in Φ_{ant} in the southern North Atlantic subpolar gyre. The negative forced response of Φ_{ant} in the subpolar gyre is the strongest in the global open ocean and is in stark contrast to the strong increasing trends seen in the regions of high per area ϕ_{ant} intensity (upper quintile integrated Φ_{ant}) (Figure 4a). These high flux intensity regions cover only 20% of the ocean but account for 40% of global Φ_{ant} in the periods 1920-1989 and

1990-2100. The highest percentile integrated Φ_{ant} from 1920-1990 is in the subpolar North Atlantic (Figure 4b). For 1990-2100, this is no longer the case, as the integrated fluxes are now arranged in a horseshoe pattern, and the highest percentile fluxes have shifted hemispheres to the Southern Ocean (Figure 4c). Timeseries illustrate the shift in anthropogenic carbon uptake from the subpolar North Atlantic to the Southern Hemisphere (Figure 5a-b). Anthropogenic carbon uptake increases linearly in the Southern Ocean (south of 45˚S) through 2070 while the subpolar North Atlantic increases at a lower rate and begins to decline shortly after 2060 (Figure 5a). As percentage of global Φ_{ant}, there is increasing dominance of the Southern Ocean (Figure 5b). In the following sections, we will identify the mechanism driving this horseshoe pattern of the forced response, and illustrate that the shift in carbon uptake intensity to the Southern Ocean can be mostly explained in the context of a reduction of the effectiveness of the North Atlantic anthropogenic carbon sink.

3.2 Relationship between Salinity and ΔpCO_2

The spatial pattern of the forced salinity trend in the subpolar gyre exhibits a similar horseshoe shape to the forced Φ_{ant} trend, with negative salinity trends present within the horseshoe (Figure 6a-b). Trends in P-E are unable to explain either the spatial pattern or the magnitude of the trend, therefore the salinity trend is likely related to changes in the circulation of freshwater. In section 3.5, we illustrate that the increase in surface freshwater comes from an Arctic source, consistent with the results from others (Holland et al. 2007, Morison et al. 2012, Vavrus et al. 2012, Koenigk et al. 2012). Regions of strong decreases in salinity south of the Greenland-Scotland Ridge (bathymetric feature at approximately 60˚N), are also regions of strongly decreasing Φ_{ant}. Henry's law dictates that ΔpCO_2, the

difference between pCO_2^{ocn} and pCO_2^{atm} (ΔpCO_2, which differs from ΔpCO_2^{ocn}, the time difference of the surface ocean pCO_2), is the dominant driver of the total carbon sink. In this region, ΔpCO_2 is negative, consistent with uptake from the atmosphere (figure 6). While ΔpCO_2^{ocn} includes changes to the natural and anthropogenic carbon cycle, because of the strong coherence between the pattern of linear trends ΔpCO_2 and the linear trends in Φ_{ant}, we are that the spatial variability in ΔpCO_2 is driven by changes to the anthropogenic carbon cycle.

Over the study period, ΔpCO_2 also exhibits a strong relationship to sea surface salinity; regions of strongly decreasing salinity are also regions of strongly increasing ΔpCO_2. In the areas with a positive trend in ΔpCO_2, or a reduction to the sea-air difference and therefore a decreasing sink, while areas of a decreasing trend are areas of a growing sink (or declining source) due to a larger difference in the partial pressures (Figure 6a,c). On monthly timescales, pCO_2^{atm} is independent of local biogeochemical processes due to the long equilibration time scale of CO_2 (months) relative to the timescale of atmospheric circulation (days). Increases in pCO_2^{ocn} must be related to the following: increases to the surface concentration of dissolved inorganic carbon (DIC), decreases in alkalinity, or increases to the sea surface temperature. On sub-centennial timescales, where climate can be considered in steady state, the natural processes controlling these variables are unable to explain long term trends. Thus, the spatial variation in the forced trend of ΔpCO_2 must be driven by spatial variation in anthropogenic changes to the physical and biogeochemical controls on pCO_2^{ocn}.

The strong surface freshening in the southern subpolar gyre could explain some of the anthropogenic change, as it would have the effect of diluting DIC and Alkalinity, which, in addition to temperature, are typically the dominant drivers of trends in pCO_2^{ocn} on decadal timescales. Dilution alone would act to decrease pCO_2^{ocn}, allowing for a more negative ΔpCO_2, and result in an increased sink (Sarmiento and Gruber, 2006). This is explained in more detail in Appendix A. However, we see the opposite relationship in this region: ΔpCO_2 is anti-correlated with salinity.

This relationship between salinity and ΔpCO_2 and air-sea flux is not unique to the CESM-LENS. In CMIP5 model simulations for 2006-2100 with RCP8.5 forcing (Figure 7a-b), a similar relationship between air-sea flux and salinity is found. Most models do not provide output for ΔpCO_2. Not only is this relationship present in other model simulations, but also the freshening of the subpolar North Atlantic is consistent between model simulations (Figure 7a). Areas that correspond to strong surface freshening, and therefore strong dilution, exhibit a strong increasing trend in ΔpCO_2, due to rising pCO_2^{ocn}. This reduces air-sea fluxes, a pattern also found in the CMIP5 results.

Yet, the negative relationship between ΔpCO_2 and salinity seen in this simulation is opposite of the increasing carbon sink surface freshening would induce alone. This indicates that other processes are changing. Candidate processes include temperature (Sarmiento and Le Quéré 1996), primary productivity (Steinacher et al. 2010, Cabré et al. 2015, Krumhardt et al. 2017) and air-sea exchange (Long et al. 2013, McKinley et al. 2016).

It is clear that the forced pCO_2^{ocn} response is not a direct result of dilution of biogeochemical properties; it must also be related to changes in the primary variables that

determine pCO_2^{ocn} (Temperature, DIC, Alkalinity, Salinity). In order to investigate the biogeochemical changes to pCO_2^{ocn}, a method that allows us to separate the effect of dilution from other physical and biogeochemical processes is required. We use the Taylor series expansion in section 3.3 to estimate the relative individual contribution of biogeochemical variables to increases pCO_2^{ocn} as well as the dilution effect.

3.3 Dominant pCO_2^{ocn} Drivers

The Taylor series decomposition of pCO_2^{ocn}, introduced in section 2.5, allows for estimation of the relative magnitude of the time change of pCO_2^{ocn} (ΔpCO_2^{ocn}) accounted for by each biogeochemical variable over the period 1992-2092. We perform this analysis for all variables that pCO_2^{ocn} is a function of, and display the results for ΔpCO_2^{ocn} due to changes in salinity normalized alkalinity (pCO_2—sAlk), salinity normalized DIC (pCO_2—sDIC), and surface freshwater (pCO_2—FW). We select only these variables for analysis because ΔpCO_2^{ocn} is mostly driven by these variables in this region. The increase of pCO_2^{ocn} due to temperature is very low in this region due to the very small projected changes in SST in the open ocean of the subpolar North Atlantic (Kay et al. 2015). Salinity normalization is performed to remove the effect of freshwater from the analysis of alkalinity and DIC changes to ΔpCO_2^{ocn}. Typically, the freshwater that is added to the surface of the open ocean comes from sources (precipitation, sea ice melt, land surface runoff) that are very low in DIC and alkalinity relative to the ocean. Surface freshwater can therefore be assumed to do very little to change the chemical properties of surface waters, and instead only acts to dilute/concentrate the chemical properties. Effectively, the addition freshwater confounds the chemical change with the physical concentration change, so we prefer to analyze its

effects separately. The linear decomposition is an approximation of the total change but provides valuable insight into the spatial variability of dominant biogeochemical variables.

pCO_2—sDIC accounts for most of the multidecadal change (1992-2092) in pCO_2^{ocn} in the study region, and is an order of magnitude greater than pCO_2—sAlk and pCO_2—FW (figure 8a-c). The large increase in pCO_2—sDIC is consistent with uptake of anthropogenic from the atmosphere driving increased surface ocean DIC. However, the rise in sDIC in the area surrounded by the horseshoe pattern, despite decreased air-sea flux of carbon, requires more in depth explanation because of the balance between air-sea flux, biological carbon export, and circulation. These factors altering the concentration of sDIC are examined in section 3.4.

pCO_2—sAlk (Figure 8b) has a much lower contribution to ΔpCO_2^{ocn} in comparison to sDIC and which is mostly due to the fact sAlk behaves in a far more conservative manner relative to DIC. Focusing our attention south of the Greenland-Scotland Ridge, we can see the roughly conservative behavior of sAlk in figure 9a where the total -17 meq m^{-3} decrease in sAlk (red dash line in figure 9a) is much less than the -83 meq m^{-3} total change due to dilution (blue dash line, figure 9a). This can be contrasted to the large change in sDIC (red dash, figure 9b). Considering the timescale of interest, the concentration sAlk is controlled by $CaCO_3$ export and circulation, with increased biologically mediated $CaCO_3$ export driving decreased sAlk at the surface. In fact, the simulation projects *decreased* export production, which indicates the decrease in sAlk is driven by circulation change. We did not investigate this further due to the small magnitude of the change.

The pCO_2—FW component is small and restricted to the area within the horseshoe (figure 8c). While dilution of alkalinity acts to increase pCO_2^{ocn}, dilution of DIC acts to decrease pCO_2^{ocn}. DIC dominates the balance (see Appendix A) so there is a slight decrease in pCO_2—FW in the southern subpolar gyre. pCO_2—sDIC is there primary contributor to ΔpCO_2^{ocn} because of the negligible contribution from other biogeochemical variables. The similarity between the spatial pattern of pCO_2—sDIC and regions of decreasing Φ_{ant} show that that pCO_2—sDIC is dominant driver of the reduced flux.

3.4 Mixed Layer sDIC Budget

Having identified pCO_2—sDIC as the principal driver of reduced air-sea carbon flux in the area enclosed by the horseshoe, we will now focus on the biogeochemical dynamics driving the increase in sDIC in the mixed layer in this area of the study region. To determine the relative importance and time evolution of the fluxes controlling mixed layer sDIC, we calculated the terms of the annual mixed layer carbon budget from monthly model output as follows:

$$\frac{d(sDIC)}{dt} = F_{circ} + F_{bio} + F_{as}$$

$$F_{bio} = -\left(\frac{\Phi_{CaCO_3}}{H_{mxl}} + \frac{\Phi_{POC}}{H_{mxl}}\right)$$

$$F_{as} = -\frac{\Phi_{as}}{H_{mxl}}$$

$$F_{circ} = residual$$

F_{bio} in our budget includes $CaCO_3$ export and particulate organic carbon (POC) export, but does not include dissolved organic carbon (DOC), which is small. The tendency of the mixed

layer carbon is calculated as the forward difference of surface sDIC. We utilize this budget to determine the source of the rise in sDIC in the region of reduced air-sea carbon flux in the southern area of the study region (south of 60˚N).

To understand how the signal inside the horseshoe varies with time, we evaluate the timeseries of F_{as}, F_{circ}, and F_{bio} at 3 locations within the subpolar gyre. Air-sea carbon flux, despite its projected decline, could still be contributing to the increase in sDIC in the mixed layer, if the projected decrease in MLD is decreasing fast enough to compensate for the decrease in Φ_{as}. Mixing in this region drives atmospheric carbon down from the surface, diminishing the accumulation in the mixed layer. A decrease in mixed layer depth would reduce the control volume (the mixed layer), and concentrate the sDIC from the air-sea flux (reducing the denominator in equation x). We see projected decreases in maximum MLD in much of the region which results in the cessation of deep mixing in parts of the Labrador Sea – a reduction of maximum MLD by more than 1500 m by 2100 (figure 10a-b). In the area enclosed by the horseshoe, however, the mixed layer carbon budget indicates a decrease in F_{as} (figure 11a-c), ruling out a compensation of the decrease in air-sea carbon by a decrease in MLD. The rate of MLD decrease (figure 10b) appears to be unrelated to when F_{as} changes and there is no a reversal of sign in F_{as} compared to the trend in Φ_{as}. With F_{as} ruled out as the explanation for increased sDIC in this region, we look to F_{circ} and F_{bio} to see if one or both of these fluxes could explain the increase in sDIC in the region of reduced air-sea flux.

We examine each sampled location (A-C) to determine the relative impact of F_{circ} and F_{bio} on air-sea flux. Location A, in the western subpolar gyre, experiences a transition

from constant F_{as} and F_{circ} in 2010, to increasing F_{circ} and decreasing F_{as}. F_{bio} is decreasing throughout the entire study period (figure 11a). The transition for F_{as} and F_{circ} occurs about a decade later (2020) at location B which is in the eastern subpolar gyre (Figure 11b). By 2070 the signal appears at location C in the Irminger Sea (Figure 11c). This signal is propagating westward, albeit at a much slower rate in the Irminger Sea. The slower rate in the Irminger Sea is likely related to the persistence of deep mixing in that area for longer than in the south of the study region (figure 10a). The deep mixing removes the advected sDIC from the surface. The propagation of the signal from east to west also suggests a source from the Davis Strait, an Arctic freshwater gateway. The coincident strongly decreasing salinity trend inside the horseshoe indicates a source of sDIC from Arctic surface water. In fact, freshwater export from the Arctic is almost entirely Arctic surface water because of the high buoyancy of freshwater relative to saltwater. Location D, within the Arctic, depicts a rapid increase in mixed layer sDIC due to F_{as} (figure 11e-g). Advective export of these waters also grows rapidly (F_{circ}). The rapid increase in F_{as} is due to reduced sea ice cover in this region, which is occurring over the Arctic as a whole, exposing the Arctic surface ocean to the atmosphere. The relatively shallow mixed layer of the Arctic concentrates the flux. Therefore, the increase in mixed layer sDIC initially occurs in the Arctic, and is advected into the study region.

The spatial pattern of changes to annual mixed layer fluxes of sDIC also show the dominance of advection in the formation of the subpolar increasing sDIC trend, but there is also an imprint of biology. As shown in figure 12b-c, F_{circ} and F_{bio} are both terms contributing to the increase in sDIC within the horseshoe. The trend in annual F_{bio} contributes to an

increase in mixed layer sDIC across the study region, but is not exceptionally pronounced in the area enclosed by the horseshoe and thus does not fully describe the spatial variability of mixed layer sDIC. The increase in sDIC due to F_{bio} is the result of less removal of mixed layer carbon by the biological pump. Increased stratification reduces mixing and entrainment of nutrients into the mixed layer, which drives reduced phytoplankton export production (Krumhardt et al. 2017). The spatial pattern of change in sDIC is primarily captured by the change F_{circ}, which indicates changes to circulation are controlling the spatial pattern of sDIC change.

Another hypothesis to consider is that the mixed layer increase in sDIC could be driven by increased sDIC below the mixed layer that is entrained into the mixed layer, but the strong stratification and shoaling mixed layers indicates that this is not occurring. Thus, horizontal advection must be supplying sDIC to the region. In the next sections, we evaluate the model's ability to simulate the export of Arctic freshwater and whether the accumulation of freshwater in the southern part of the study region is from an Arctic source.

3.5 Comparison of Modeled Arctic Freshwater Export to Observations

In the model, Arctic freshwater can enter the North Atlantic through the three major Arctic freshwater gateways: Davis Strait, Fram Strait, and Barents Sea Opening (Figure 1). The only freshwater gateway that the model does not represent is the Fury and Helca strait, which connects Hudson Bay to the Arctic. This gateway offers a negligible contribution to the total freshwater export from the Arctic (Aagard and Carmack 1989). There exists large interannual variability in trends in Arctic freshwater content which makes the ensemble

mean alone a poor comparison to observations. This has been discussed with respect to sea ice area in Swart et al. (2015). Comparisons to observations are listed in table 3.

In the Davis Strait, the model agrees well with the observed vertical salinity structure and observed seasonal variability over the period 2004-2010 analyzed by Curry et al. (2014) (Figure 14). We consider the ensemble able to accurately produced natural variability within the strait, if the confidence interval of the observations overlaps with the 95% confidence interval of the ensemble mean. The -93 ± 6 mSv observed by Curry et al. (2014) during this period is outside the confidence interval of the ensemble mean, -73 mSv ± 2. The ensemble mean solid freshwater transport is -23 mSv ± 0.4 is also outside of the confidence limits of the observed transport of -10 ± 1 mSv. However, together, these yield a net freshwater transport of 98 ± 2 mSv, well within the uncertainty of the observed -103 ± 7 mSv.

In the Fram Strait, in the CESM-LENS the liquid freshwater export is only -4 mSv ± 0.4 mSv compared to the observed mean transport of - 84 ± 16 mSv (95% less) for 1992-2001 (Jahn, 2012). In this strait, the modeled salinity field in the shelf region is much more saline than observed (De Steur et al. 2009). The very low modeled freshwater transport is possibly due to a weaker than observed northward flowing west Spitsbergen Current (WSC). In addition, the model has a northward undercurrent along the East Greenland Shelf that is not observed. The undercurrent transports freshwater into the Arctic, thus reducing the net export. Increased model resolution could lead to a more accurate representation of the current structure (Hatterman et al. 2016). The CESM-LENS captures the observed solid freshwater export well, with -89 mSv ± 3 annually compared to an observed value of -73 ±

11 mSv. The CESM-LENS net transport of -93 ± 3 mSv is 59% of the observed net transport, -157 ± 27 mSv. The low CESM-LENS liquid freshwater export through the Fram Strait is a major contributor to the clearly low net transport of freshwater through the Fram Strait.

The modeled Barents Sea Opening contributes a very small amount of freshwater to the North Atlantic, which is consistent with observations (Jahn et al. 2012): -3 mSv solid (model), -1.2 mSv solid (obs.), -0.1, mSv (model), -2.9 ± 3.0 mSv liquid (obs.). The CESM-LENS values do fall within the large uncertainty on the net transport.

3.6 Increasing Arctic Freshwater Export

Considering the study region as a whole, there are increases in liquid freshwater towards the end of the century (figure 15a), but those increases are counteracted by decreasing solid freshwater export (sea ice) (figure 15b). Decreasing solid freshwater export in CESM-LENS is due to the reduction in Arctic sea ice. Net freshwater (solid + liquid) export does increase through the Davis Strait, greatly reducing salinity and alkalinity, while maintaining constant DIC despite dilution (increased sDIC) in the are enclosed by the horseshoe region (Figure 9a). Despite this increase, there is no significant net trend in net Arctic freshwater export to the North Atlantic in CESM-LENS, counter to previous modeling results (figure 15c) (Holland et al. 2007, Morison et al. 2008, Vavrus et al. 2010, Koengigk et al. 2012). The difference in the partitioning of freshwater East or West of Greenland does not drastically alter the result as seen by the comparison of CESM-LENS to CMIP5 (figure 7a).

Arctic freshwater is the locally dominant source of freshwater in southern subpolar gyre compared to decreases to the P-E ratio (figure 16) and slight increase in runoff (Figure

17). This suggests that in regions where there are positive trends in ΔpCO_2, and increasing sDIC, that this is related to freshwater forcing from the Arctic, rather than local processes. The freshening is restricted to the surface layers due to the lower density of freshwater and it is in the upper layers of the ocean where the change in surface water biogeochemical properties, in this case enhanced advection of Arctic mixed layer carbon, can have a large impact on air-sea exchange. This indicates a strong mechanistic coupling between the high latitude North Atlantic carbon sink and the hydrological cycle of the Arctic.

4. Physical Interpretation of the Salinity Normalized Results

The separation of freshwater from biogeochemical effects is useful for identifying the driving mechanisms of biogeochemical changes to ΔpCO_2^{ocn} and can be considered in the physical context of the effects of raw DIC and alkalinity on air-sea exchange. We relate the salinity normalized results to DIC and alkalinity because the raw values are what actually impact pCO_2^{ocn} and the air-sea exchange of carbon, by altering the buffer factor. In the southern section of the study region we see that DIC is increasing, while the alkalinity decreases strongly (figures 9a-b). Our results show that the decrease in alkalinity is due to dilution of sea surface alkalinity by surface freshwater. The increase in DIC is due to advection of carbon absorbed from the atmosphere into the Arctic mixed layer into the study region, which overwhelms the effect of dilution as shown by our linear analysis and mixed layer sDIC budget. The reduced air-sea exchange is therefore primarily due to an increase in DIC, with this effect exacerbated by the decrease in alkalinity, greatly altering the buffer factor. The decline in alkalinity and the increase in DIC is ultimately due to

expansion of Arctic surface water into the subpolar gyre as these biogeochemical properties are advected along with the Arctic surface freshwater.

5. Discussion

There are many uncertainties with regard to the freshwater flux into the region. Like most climate models, CESM-LENS has fixed ice sheets. This choice is made because models of glacier surface mass balance are not currently advanced enough and lack in-situ observations to compare to. In CESM-LENS, the only freshwater that may be contributed to the region from the Greenland Ice Sheet is runoff – the Greenland Ice Sheet itself is static. Increases in basal melting due to increasing ocean temperatures may result in increasing ice mass flux from the Greenland's glaciers (Rignot 2011). Response of Arctic freshwater content, its distribution and the magnitude of release to the North Atlantic, remain unceratain. A combination of uncertainties regarding the accuracy of simulated wind patterns, the hydrological cycle, sea ice, all open up a possibility that the increasing freshwater flux to the high latitude north Atlantic could be greater than what we have currently modeled (Haine et al 2015). These uncertainties have, in part, motivated model experiments that subject the region to very high fluxes of freshwater (Stouffer et al. 2006, Swingedouw et al. 2013) to assess physical effects. If freshwater is released to the North Atlantic at a higher rate than projected here, the stratification could be greater in this region and expansion of the decreased flux signal would be expected.

The general concept of freshwater affecting surface ocean pCO_2 is not new, however the direct link between advection of freshwater proposed here and should not be confused with the dilution/concentration mechanism that is normally associated with freshwater.

Keeling et al. (2004) observed how changes in the freshwater budget could increase pCO_2 at Station ALOHA, the site of the Hawaii Ocean Timeseries (HOT) program over 14 years. In this case there was a decrease in surface freshwater flux, leading to an increase in alkalinity. Rather than driving pCO_2 downwards due to increased buffering capacity, there was an increase pCO_2 because of the resulting increase in DIC, overwhelmed the decrease in pCO_2 caused by high alkalinity concentrations. In most instances, when the increase in surface freshwater is directly linked to the balance between precipitation, dilution/concentration of DIC would dominate

CESM-LENS indicates a different response to surface freshwater in the North Atlantic because DIC remains constant in the regions with strongly decreasing trends alkalinity. The advection of sDIC along with surface freshwater, while sALK remains constant, overwhelms the effect of dilution and maintains constant DIC in the region within the horseshoe while there is little change to sAlk and therefore Alkalinity is strongly diluted by the freshening. Constant DIC in the presence of decreasing alkalinity drives pCO_2 higher, as evidenced by our linear ΔpCO_2^{ocn} analysis, and drives the reduction of the anthropogenic air-sea flux of carbon.

As earth system models improve, prognostic riverine fluxes of nutrients will be introduced and will require modifications to the linear ΔpCO_2^{ocn} analysis in this region because of the large river contribution to surface freshwater (Aagard and Carmack 1989, Yamato-Kawai et al. 2009). In CESM-LENS, as in most earth system models, inputs of surface freshwater (riverine, precipitation) occur without the addition of alkalinity or DIC, but the freshwater fluxes from rivers certainly do contain both of these biogeochemical

variables (Dittmar and Kattner 2003). Understanding how the shelf ecosystem modifies riverine nutrient fluxes along the broad continental shelf is another process where our understanding is limited. Theoretically, nutrients introduced by rivers could be largely consumed at the continental margin, but such affects are not typically modeled. A simple but computationally expensive way to preserve the utility of this method would be to use model tracers to differentiate between freshwater sources and nutrients from an oceanic source or riverine source – then the experimenter could normalize for freshwater accordingly. The absence of riverine nutrient input permits the usage of our linear ΔpCO_2^{ocn} analysis, but the addition of these processes would complicate the implementation of this technique.

6. Summary and Conclusion

The CESM-LENS indicates that Arctic freshwater export could play a significant role in future reduction of the intensity and magnitude of the high latitude North Atlantic carbon sink (figure 18). Increases in freshwater in the Arctic drive increasing surface freshwater flux into the region. The increase surface freshwater dilutes alkalinity and while advection of an increasing concentration of sDIC from the Arctic overwhelms the dilution effect. The net effect is an increase in DIC and a decrease in alkalinity, which increases surface ocean pCO_2 at rate faster than the growth of atmospheric pCO_2, driving a reduced uptake of anthropogenic carbon in the North Atlantic. We base this claim on the pCO_2—sDIC contribution over the study period being large in comparison to pCO_2—sAlk, a relationship we find in regions of strongly increasing trends in ΔpCO_2. The end result is a transition from

the subpolar North Atlantic being one of the most intense sinks of anthropogenic carbon, to the Southern Ocean assuming the highest anthropogenic carbon flux density.

The drastic changes to circulation in the region also alters the carbon cycle regionally. These changes could be linked to the increasing Arctic freshwater export to the subpolar gyre, with the strongest possible relationship being the reduction of MLD and diminishing area of modeled deep water formation sites due to freshwater induced positive buoyancy flux. These changes to mixing result in decreases to the biological pump and exacerbate the increase in sDIC. Future work could be done to improve the mixed layer carbon budget by explicitly calculating advection. The standard configuration of the CESM for the CESM-LENS project did not output these variables, but the advection terms for sDIC could be saved if one were to run their own simulation.

Climate change is driving freshwater export and interacts with the North Atlantic carbon cycle in what is clearly a climate-carbon feedback. Future work using a different experimental design and additional model simulations could be used to estimate the sensitivity of carbon to climate change in this region. We would expect the sensitivity to warming to be very high, similar to what is shown in Randerson et al. (2015). With three simulations, an idealized 1% per year increasing CO_2 (1% CO_2) simulation, a radiatively uncoupled 1% CO_2 simulation, and constant climate control simulation, I would be able to quantify the magnitude of the loss of carbon uptake due to climate change. The impacts of reduced Atlantic Meridional Overturning Circulation (AMOC) could also be examined in this framework. This experimental design is the necessary next step for quantitatively determining the loss due to climate change in this region.

Observations in the subpolar North Atlantic and Arctic will remain necessary to monitor regional climate change, improve our understanding of the Earth system, and inform our model projections. Our understanding of the interaction between Arctic ocean and land biogeochemical processes remains limited, which limits its inclusion in earth system models, and contributes to the uncertainty regarding the degree to which large future increases in the export of terrigenous carbon and other nutrients could impact the carbon cycle of the Arctic and subpolar North Atlantic (Dittmar and Kattner 2003). For observations of river discharge and biogeochemistry, which could be used to constrain model estimates of nutrient flux to estuaries, the short length of record of observations, lack of long term sampling of the full seasonal cycle, and the riverine measurements often being only single point measurements, results in limited insights into the controlling biogeochemical mechanisms. Coordinated observations of Arctic river discharge and biogeochemical properties only first began with Arctic Great Rivers Observatory (Arctic-GRO) in 2002 and continuous observations began even later at most of the Arctic-GRO observation locations. The continued funding of Arctic-GRO is important but understanding river discharge and its biogeochemical properties are insufficient in isolation, and because of the possibly far reaching effects, need to be partnered with ocean biogeochemistry studies that focus the fate of the nutrients that are exported to the Arctic ocean, and eventually to the Atlantic through the same pathways as Arctic surface freshwater. We could improve our confidence in the magnitude of the modeled climate-carbon feedback driven by Arctic freshwater by leveraging the existing observational framework of the Overturning in the Subpolar North Atlantic Program to provide confirmation of our

modelling results, but that would require new instrumentation. Since 2014, the OSNAP array has monitored the deep overturning circulation in the subpolar gyre, but biogeochemical observations are not integrated. Adding oxygen and pCO_2 observations to OSNAP could improve our understanding of the carbon cycle in the subpolar gyre by providing fully resolved seasonal cycles of pCO_2 and we eventually assess long term trends. Volunteer observing of pCO2, biogeochemical ARGO floats, continued repeat hydrographic observations, and further modeling studies in the North Atlantic are also critical. Continued improvements to our earth system models and the accuracy of their projections are dependent on ongoing and continuous observations in the subpolar north Atlantic and Arctic.

Tables and Figures

Table 1

Sea Surface Salinity	CO_2 Flux	ΔpCO_2
ACCESS1.0		
ACCESS1.3		
CMCC-CESM	CMCC-CESM	
CNRM-CM5	CNRM-CM5	CNRM-CM5
CanESM2	CanESM2	CanESM2
GFDL-CM3		
GFDL-ESM2G	GFDL-ESM2G	GFDL-ESM2G
GFDL-ESM2M	GFDL-ESM2G	GFDL-ESM2G
GISS-E2-H-CC	GISS-E2-H-CC	
GISS-E2-R-CC	GISS-E2-R-CC	
HadGEM2-ES	HadGEM2-ES	
IPSL-CM5A-MR	IPSL-CM5A-MR	IPSL-CM5A-MR
MIROC-ESM-CHEM	MIROC-ESM-CHEM	
MIROC5		
MPI-ESM-MR	MPI-ESM-MR	MPI-ESM-MR
	MPI-ESM1	
NorESM1-ME	NorESM1-ME	

Various simulations we selected and the variables from those simulations provided by ESGF. More accurate model diversity is depicted by excluding some of the available simulations (Table 2).

Table 2

No Carbon/Ecosystem	Low Resolution Variant	Performance
CMCC-CM	IPSL-CM5A-LR	INM4-CM4
CMCC-CM5	IPSL-CM5A-LR	
GISS-E2-R	IPSL-CM5B-LR	
GISS-E2-H	MPI-ESM-LR	
HadGEM2-AO		
HadGEM2-CC		
MIROC-ESM		
NorESM1-M		

Cause for the exclusion of an available simulation. The INM4-CM4 is the only model excluded due to performance.

Table 3

Gateway	Modeled Liquid	Observed Liquid	Modeled Solid	Observed Solid
Davis Strait (2004-2010)	-74 mSv ± 2	-93 ± 6 mSv	-23 mSv ± 0.4	-10 ± 1 mSv
Fram Strait (1992-2001)	-4 mSv ± 0.4	-84 ± 16 mSv	-89 mSv ± 3	-73 ± 11 mSv
Barents Sea Opening (1992-2001)	-0.1, mSv	-2.9 ± 3.0 mSv	-3 mSv	-1.2 mSv solid

Comparison between modeled and observed freshwater transport. Estimates for transport come from Curry et al. (2014) for the Davis Strait and Jahn et al. (2012) for the Fram Strait and Barents Sea Opening

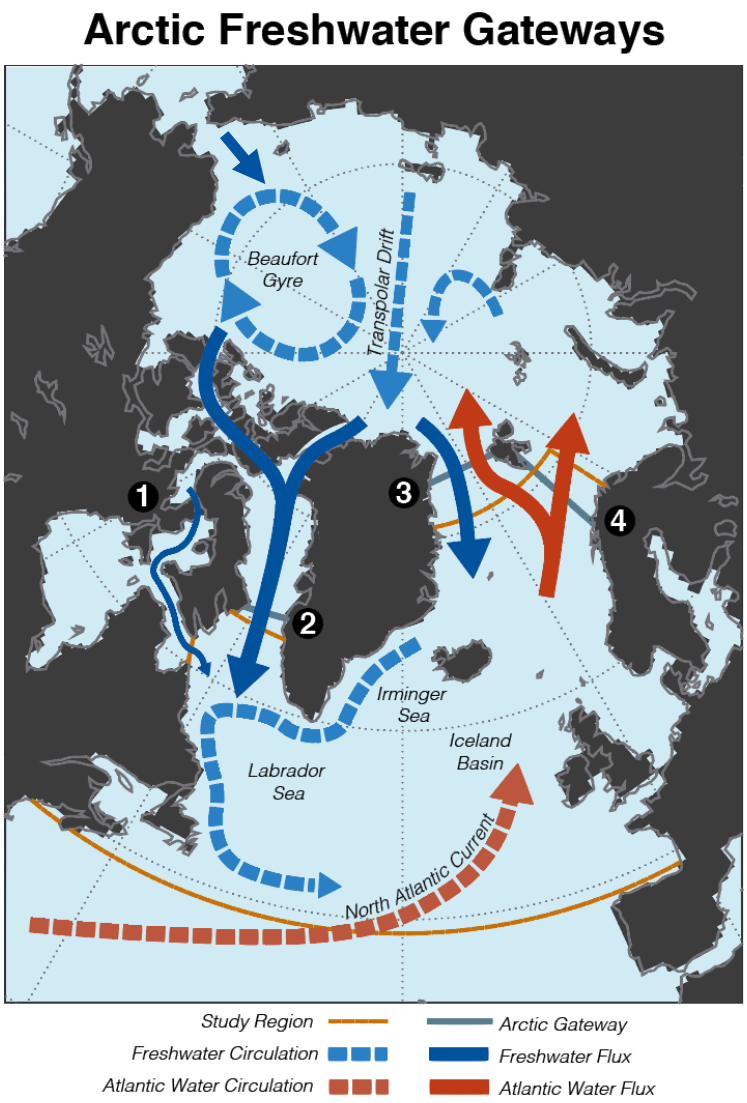

Figure 1: The pathways along which Atlantic water (orange dotted line) and freshwater (blue dotted line) are circulated with the gyre. Solid red lines indicate the pathways for these water masses to enter/exit the Arctic. The straits where freshwater enters or exits the region are denoted with numbers, from east to west. They are the Fury and Helca Strait (1), Davis Strait (2), Fram Strait (3), and Barents Sea Opening (4). Of these, most of the Arctic freshwater is observed to enter the North Atlantic through the Fram and Davis Straits.

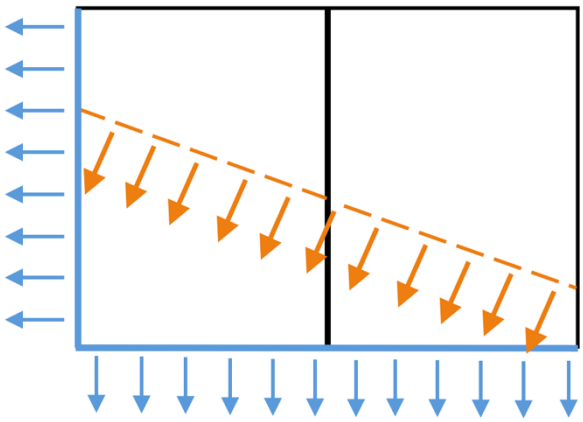

Figure 2: Transport is calculated with two different methods. The two boxes represent the faces of grid cells and the orange dotted line represents the method for calculating liquid freshwater flux. The blue highlighted faces are the faces along which the model fluxes freshwater, and what is used for the calculation of solid freshwater flux.

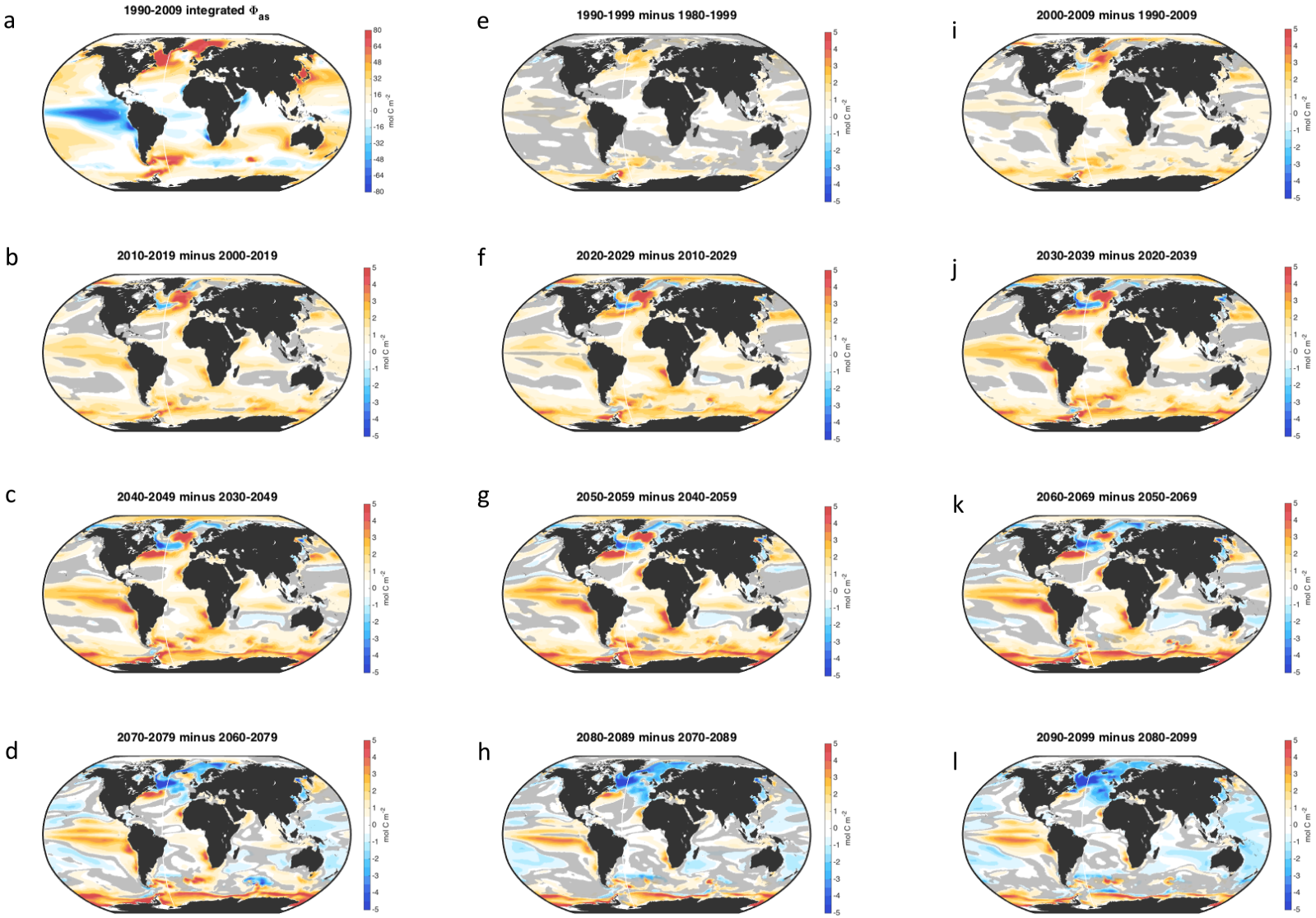

Figure 3a-l: A) the pattern of integrated air-sea exchange (Φ_{as})over the first 20 years of the study period. B-L) the decadal difference from 1990 to 2099. The shading indicates regions of insignificance (outside 95% ci). Note strongly decreasing flux in the subpolar N. Atl.

a

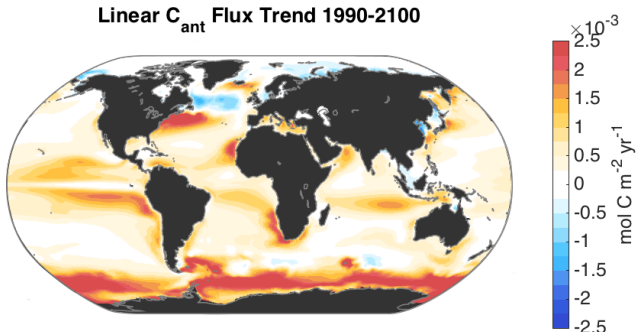

b

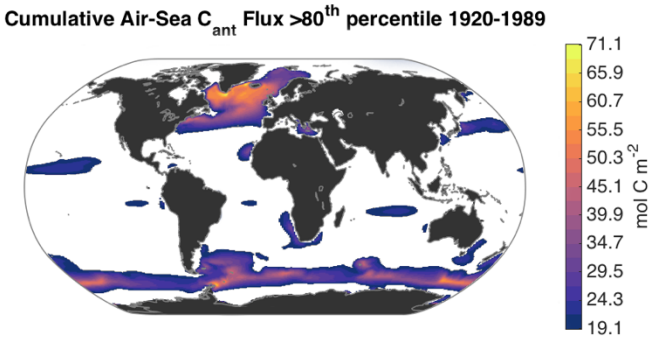

c

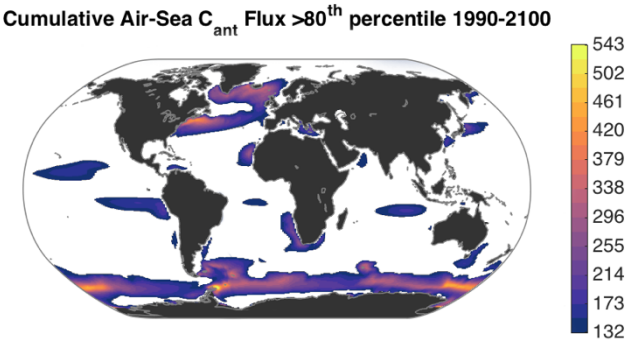

Figure 4a-c: (a) There is a decreasing trend in air-sea anthropogenic carbon flux in the North Atlantic. This trend is the strongest globally in the open ocean. (b) 1920-1989 the subpolar N. Atlantic was the most intense region of integrated anthropogenic carbon uptake, nearly the entire area within the upper quintile of flux intensity (mol C m^{-2}). (c) 1990-2100, the upper quintile of integrated fluxes has shifted into a “horseshoe” pattern.

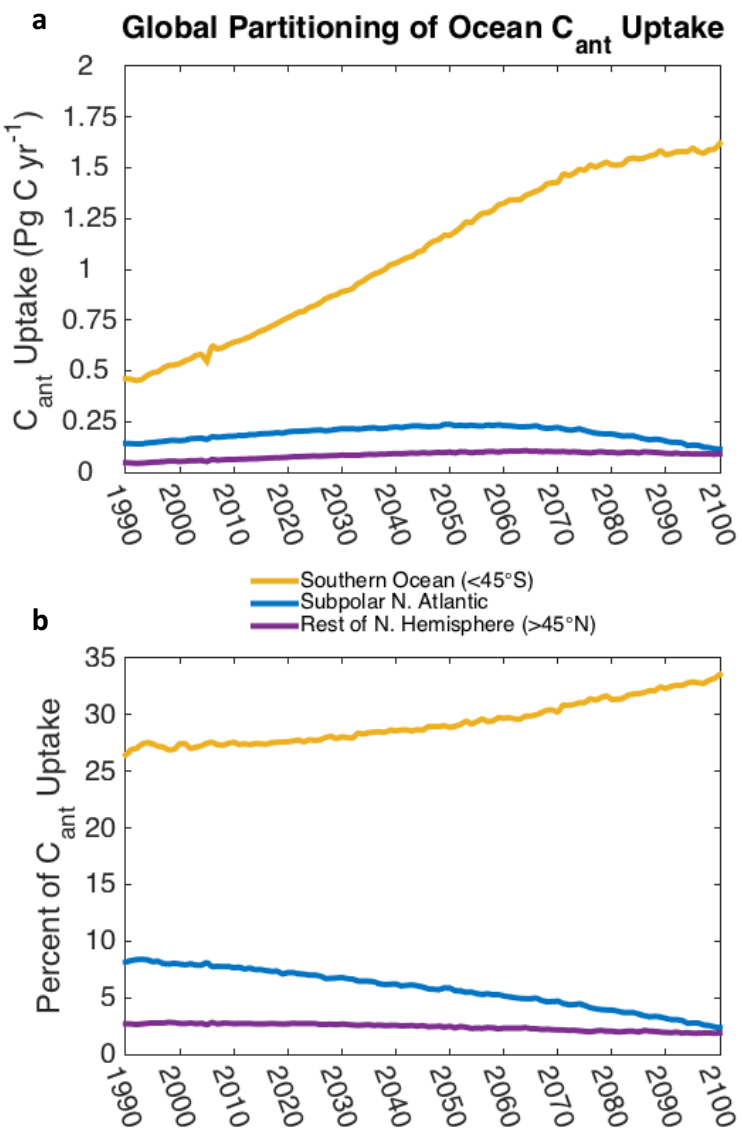

Figure 5a-b: (a) Rapid increase in S. Ocean (< 45˚S) anthropogenic carbon uptake (C_{ant}) compared to an eventual decline in the study region. (b)The subpolar North Atlantic is steadily decreasing in percentage of global C_{ant} uptake

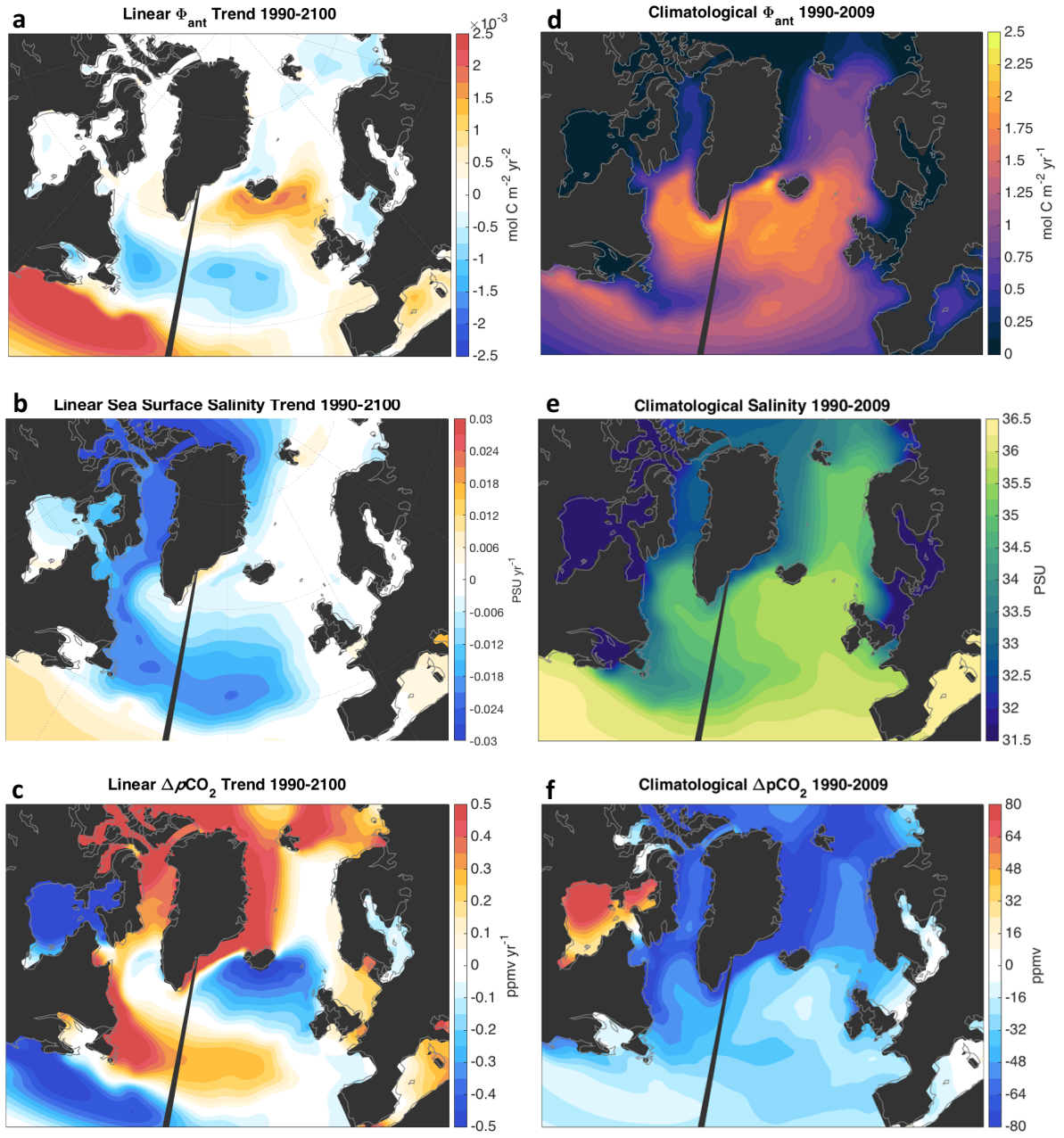

Figure 6a-f: The spatial pattern of the (a) annual anthropogenic uptake trend is surprisingly similar to the (b) linear trend in salinity. The spatial pattern of the (c) linear ΔpCO_2 trend is also similar. Regions of decreasing flux trends are driven by increasing ΔpCO_2. This suggests that surface freshwater may be altering the carbon cycle by change pCO_2^{ocn}. (d-f) climatological values for these variables. A

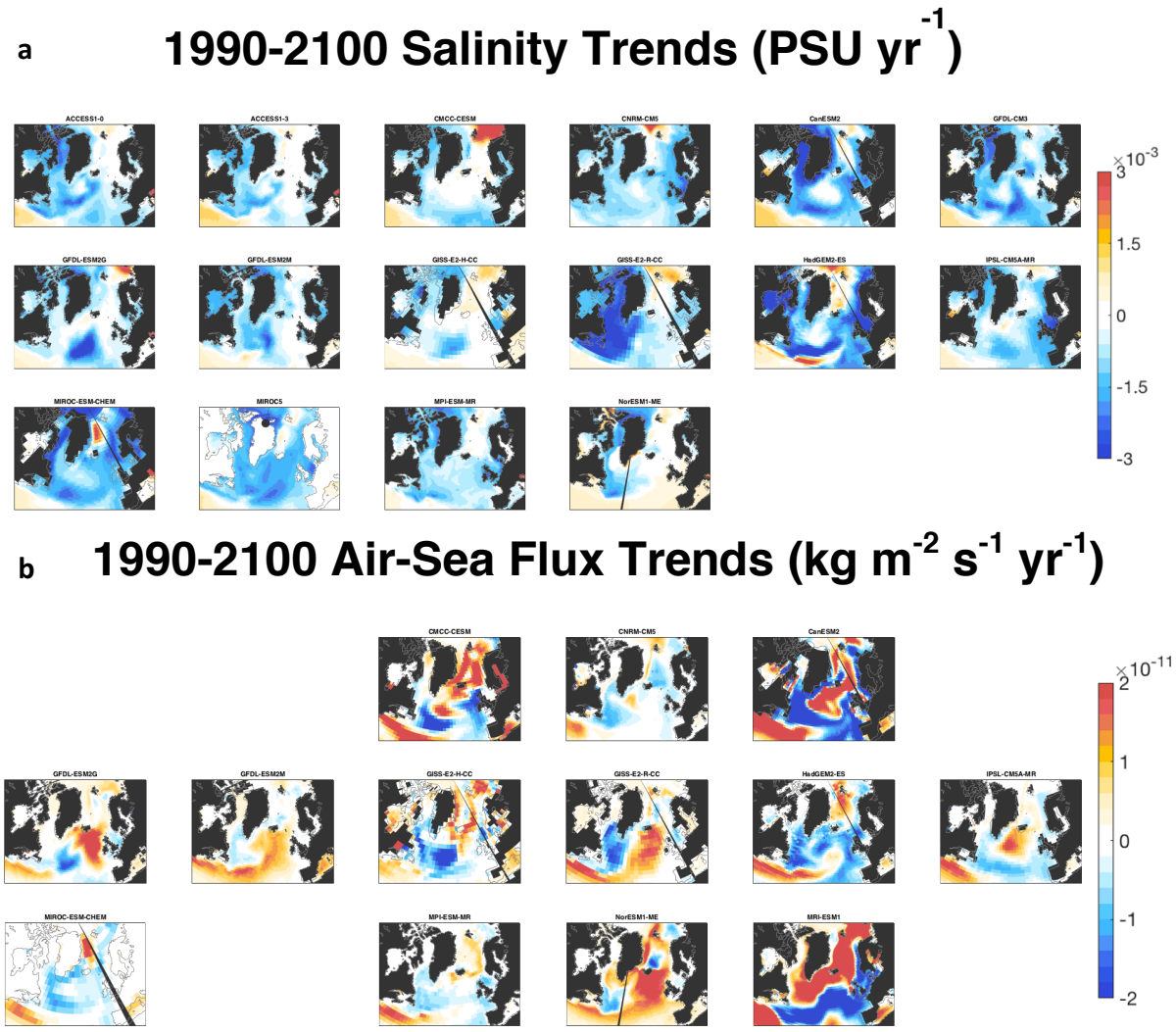

Figure 7a-b: Linear trends of simulated (a) salinity (PSU yr^{-1}) and (b) air-sea flux (kg m^{-2} s^{-1} yr^{-1}) from CMIP5 models. All models project surface freshening the subpolar gyre and show coincident decreased flux, although the strength of this relationship varies model to model. Table 2 lists the models used and why certain models were excluded from this study

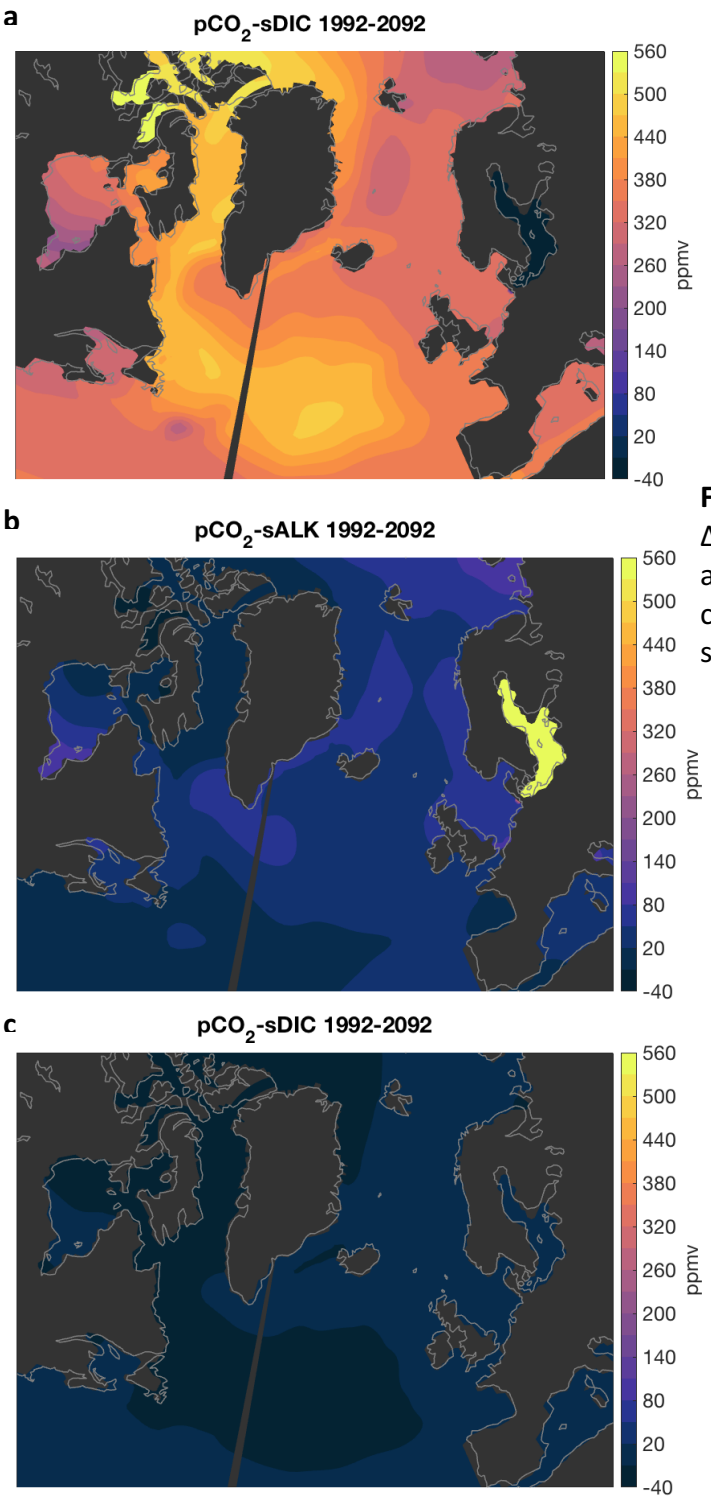

Figure 8a-c: Results from the linear ΔpCO_2^{ocn} analysis. ΔpCO_2^{ocn} changes are separated into changes due to change in (a) sDIC, (b) sALK and (c) surface freshwater (FW).

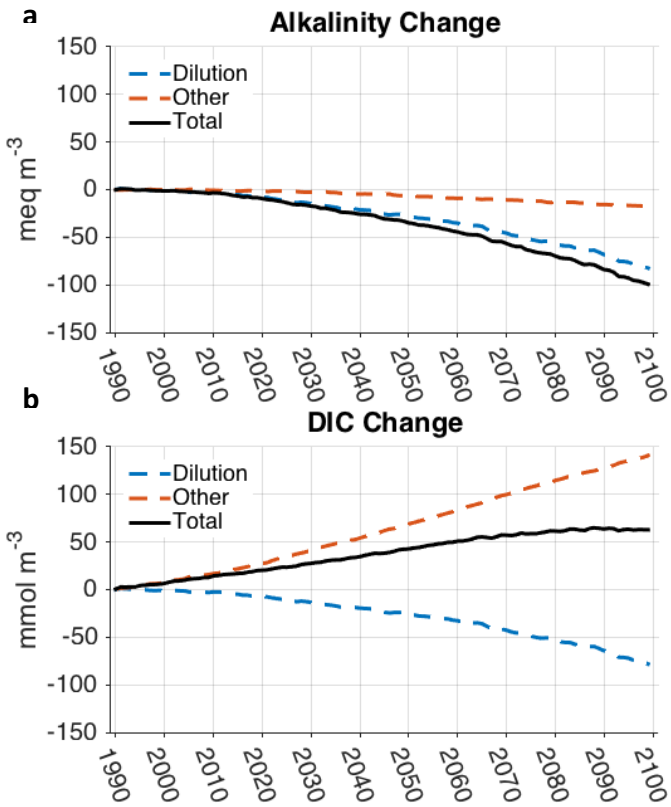

Figure 9a-b: Using the linearization of equation 3, average over a latidudinal box between 44˚N and 60˚N, (a) total change in surface DIC (black line) and the dilution and all other changes (blue and orange dashed lines, respectively), with same for (b) surface alkalinity.

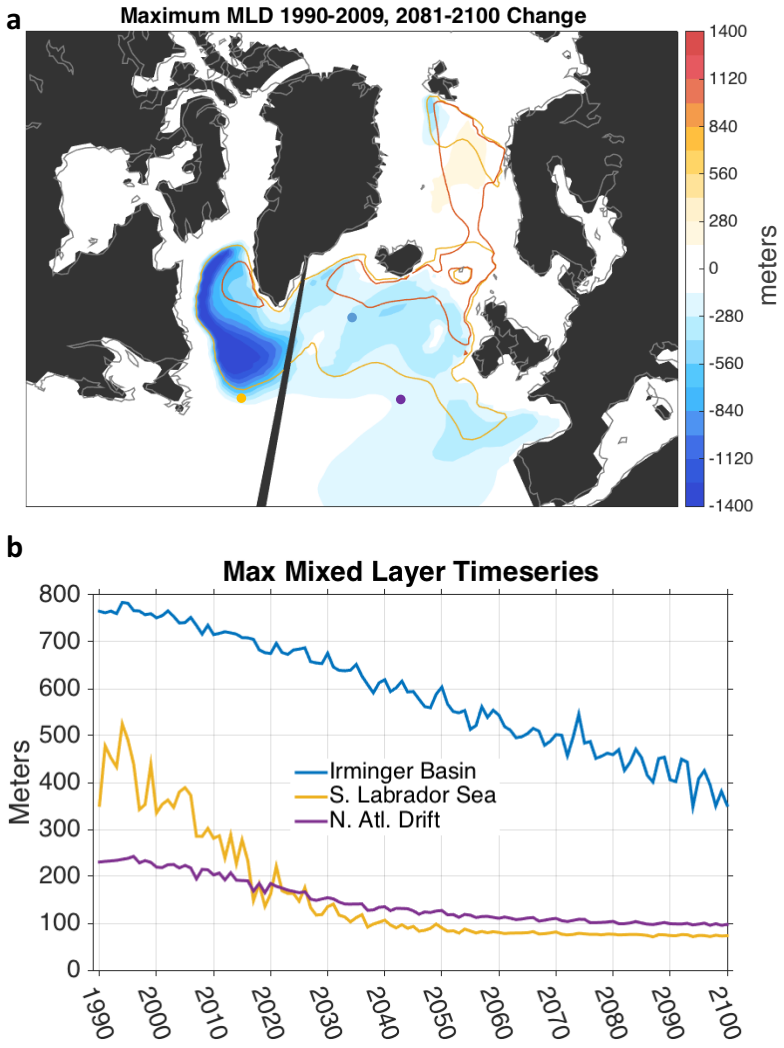

Figure 10a-b: Warming induced stratification, and then capping by freshwater, results in the (a) cessation of deep mixing in the southern Labrador Sea. Filled contours represent the change in the annual maximum MLD (meters). The yellow contour is the annual average maximum MLD 1990-2009, while the orange contour is the same but for 2081-2100. This depicts a northward shift of mixing. The colored dots in 10a represent location of the (b) timeseries and the colors used for the dots correspond with colors of the lines in the timeseries. The most rapid change in mixing is in the South Labrador Sea.

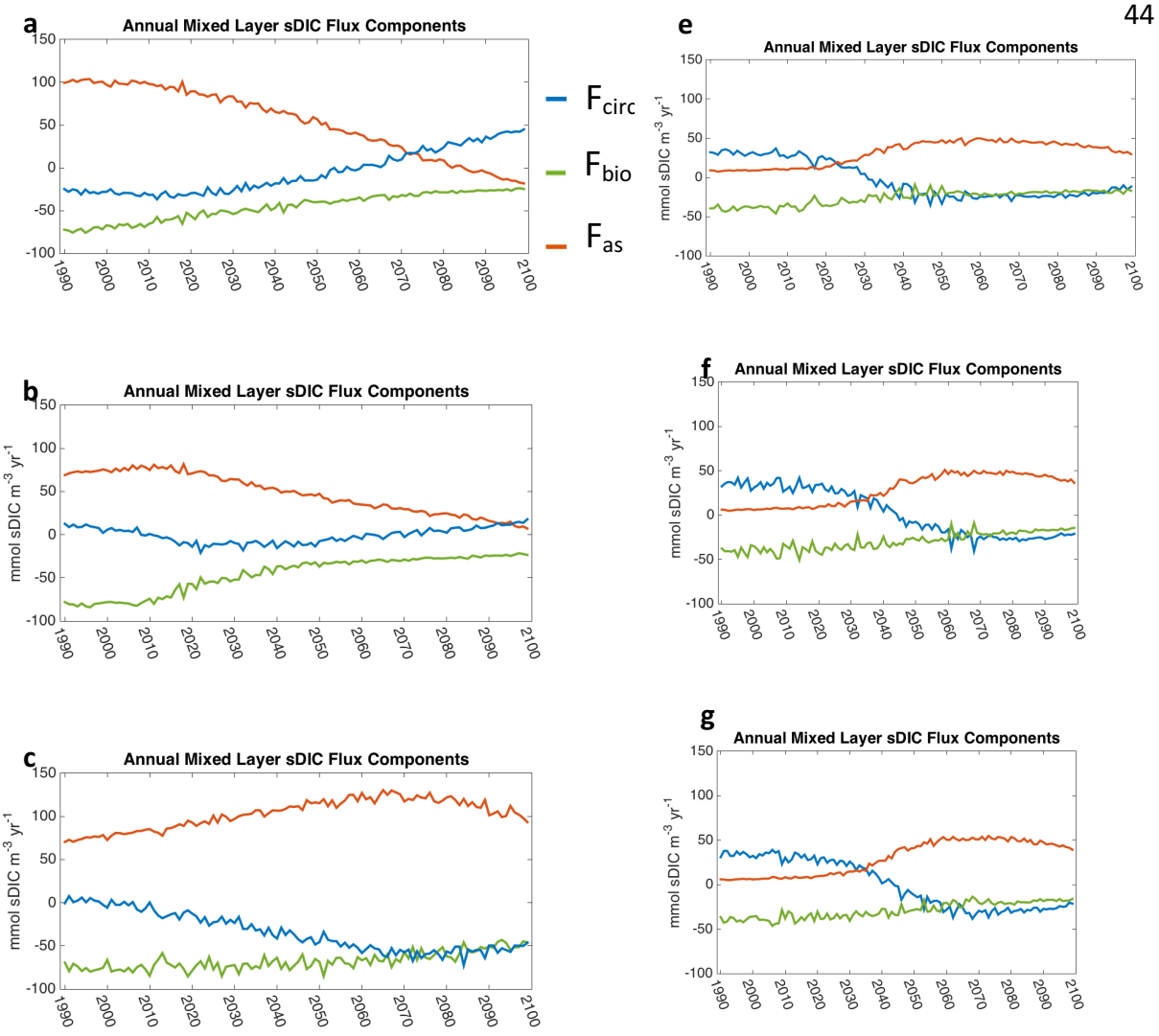

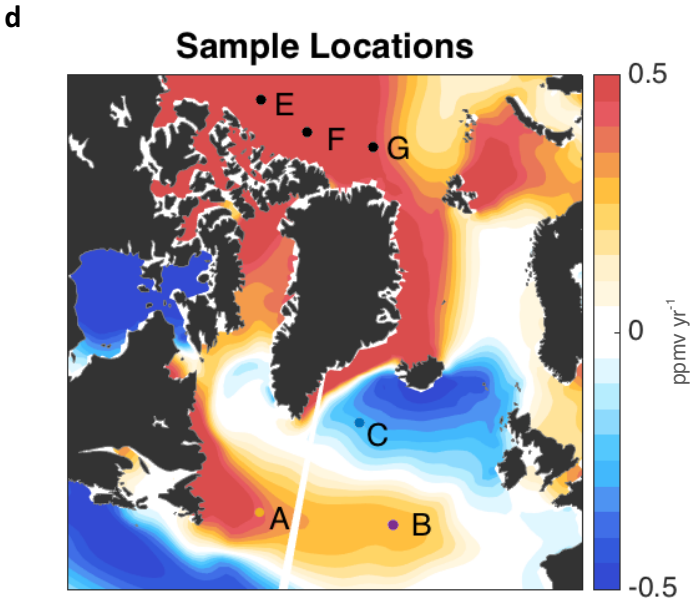

Figure 11a-h: (a-h) Timeseries of the mixed layer budget terms. (d) location relative to the positive trend in ΔpCO_2 where each of the time series are sampled from. These figures would be improved with inclusion of the natural variability, like the freshwater figures.

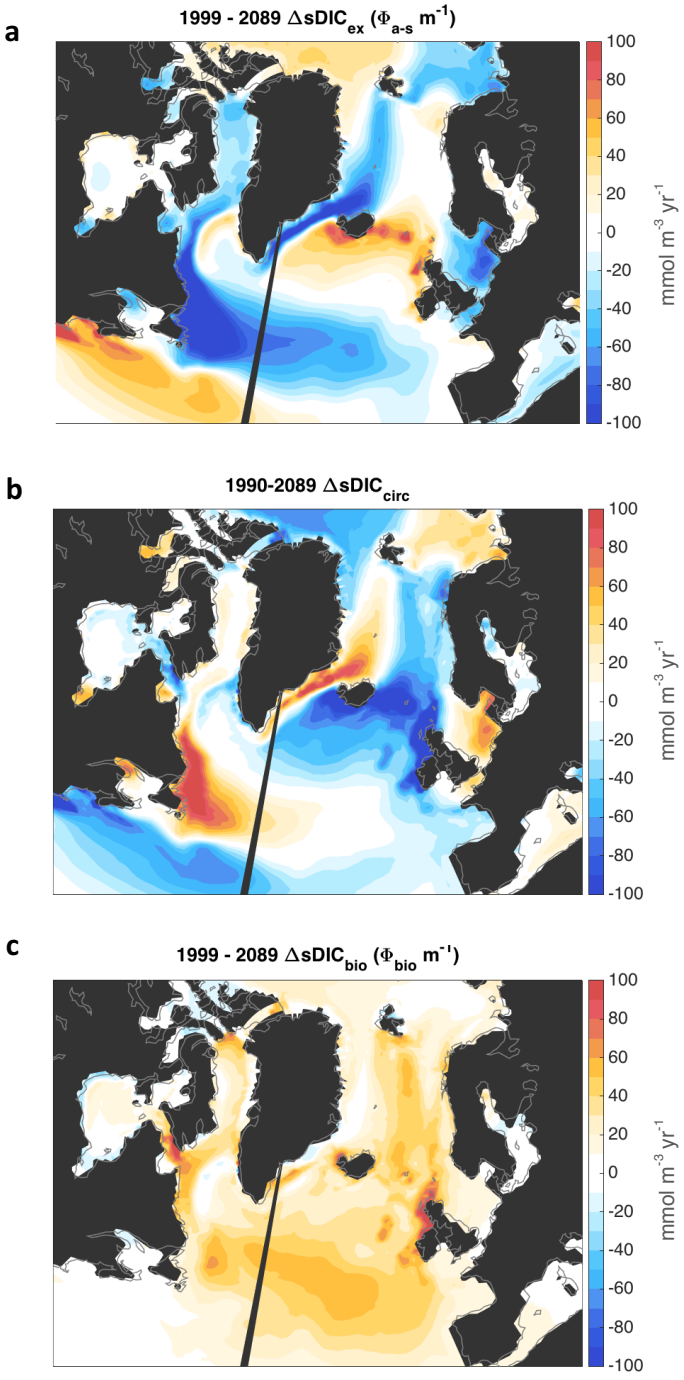

Figure 12a-c: Differences between the annual mixed layer sDIC terms (mmol m^{-3} yr^{-1}): (a) change in mixed layer sDIC due to air sea exchange (F_{as}), (b) circulation (F_{circ}), and (c) biology (F_{bio}).

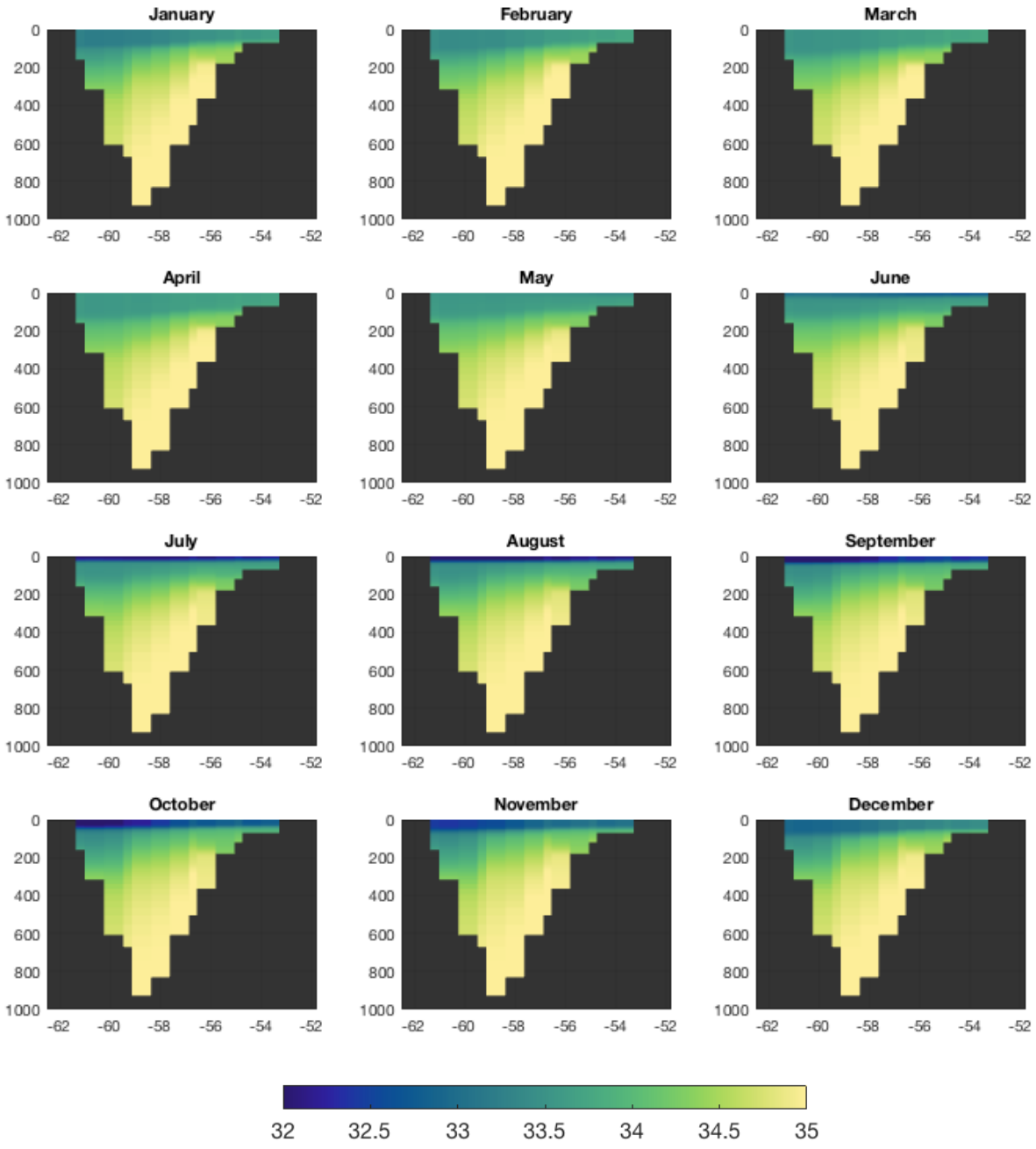

Figure 14: Mean monthly salinity for ensemble member 1 with the same study period 2004-2010 of Curry et al. (2011) (see their figure 3). The x-axis is longitude. The model is more diffuse than observations, but it generally has the same salinity structure and seasonal variability. Sea surface salinity reaches is lowest Aug-Oct, and highest in January. The waters at depth are saltier towards Greenland (east) and fresher towards Labrador (west). This similar to what was observed by Curry et al. (2011).

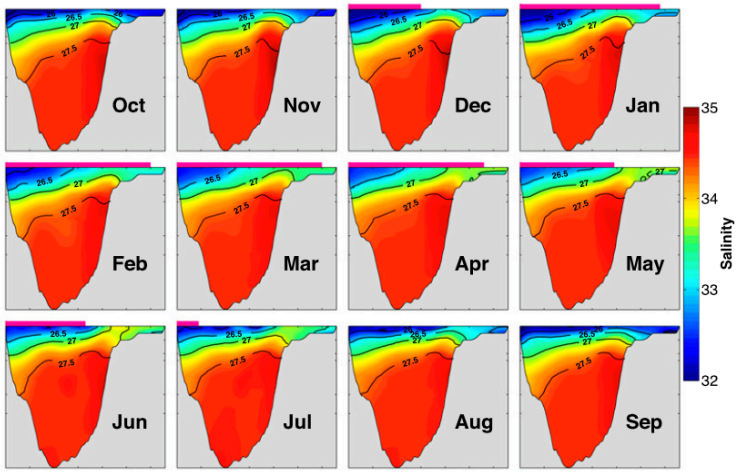

Figure 3 (Curry et al. 2011): monthly averages of salinity (shading) with potential density contours

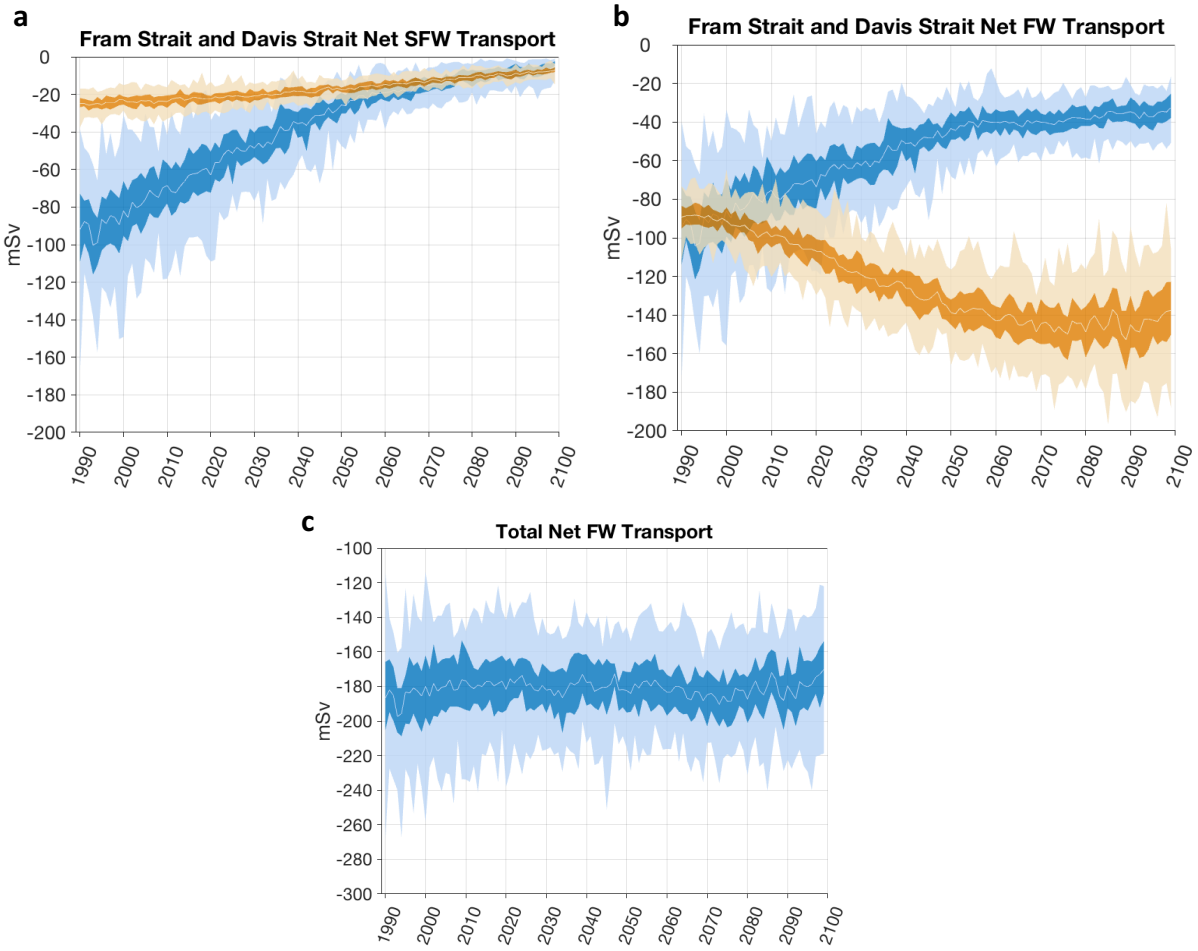

Figure 15a-c: Annual timeseries of Fram Strait (Blue) and Davis Strait (Orange) (a) solid freshwater export, (b) net (solid + liquid) freshwater export, and (c) in blue, total Arctic freshwater export to the region (Fram Net + Davis Net). Light line is the ensemble mean, dark shading denotes the interquartile range, and light shading is the ensemble max/min.

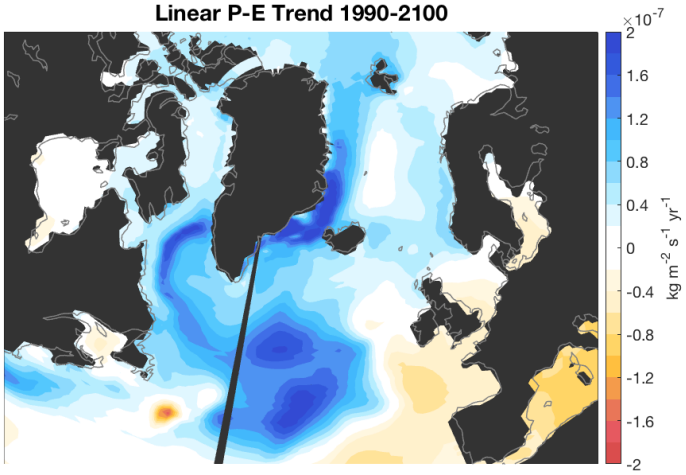

Figure 16: Linear trend in precipitation (kg m^{-2} s^{-1} yr^{-1}). Blue (red) regions are regions of increasing (decreasing) precipitation and/or decreasing (increasing) evaporation, representing the addition of freshwater to the ocean.

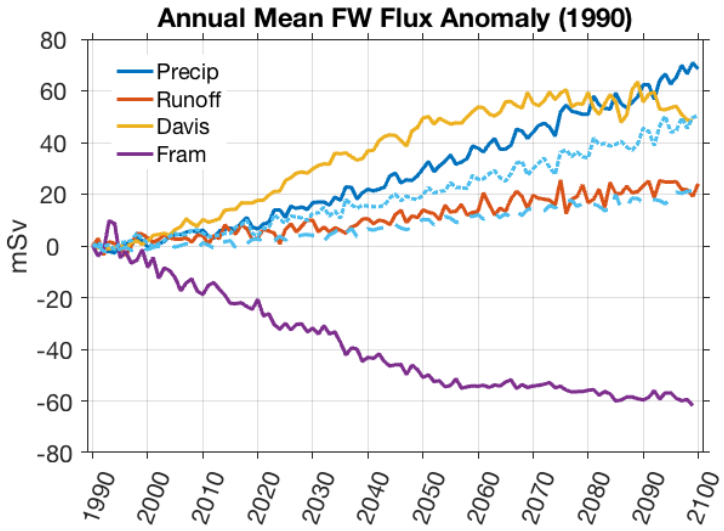

Figure 17: Timeseries of various sources of freshwater anomalies relative to 1990 (mSv). The solid blue line represents net precipitation (precipitation-evaporation). The dashed blue line represents net precipitation north of 60˚N and the dotted blue line represents net precipitation south of 60˚N. The Davis strait (yellow line) and Fram Strait (purple line) are the largest freshwater anomalies, indicating their dominant role in the freshwater balance of the northern and southern subregions of the study region.

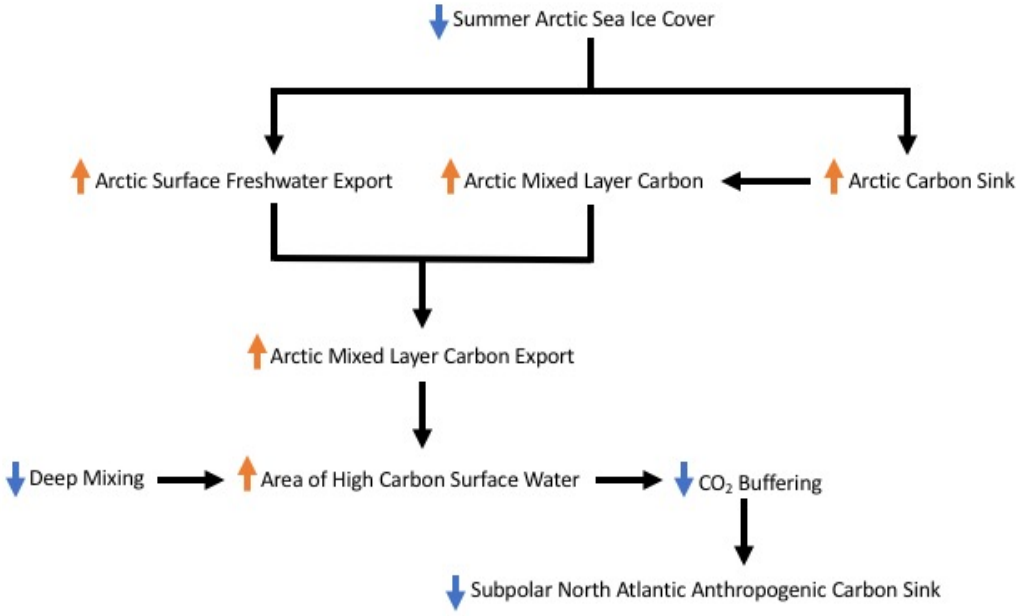

Figure 18: Schematic diagraming the interaction of processes that lead to a reduced North Atlantic Carbon sink and the formation of the horseshoe pattern. The orange and blue arrows in this simplified diagram indicate the direction of change caused by these interactions

Appendix A

The solubility of CO_2 in water can be described as the concentration of carbonic acid ($[H_2CO_3^*]$) divided by the solubility constant for CO_2, k_0:

$$pCO_2 = \frac{[H_2CO_3^*]}{k_0} \qquad eq.\ A1$$

In seawater, the concentration of carbonic acid is a very small component of the total concentration of inorganic carbon (DIC). Dissolved CO_2 rapidly undergoes multiple reactions upon entering seawater, and the final concentration is controlled by the speciation (distribution of elements in a chemical system) of dissolved CO_2 into carbonate and

bicarbonate ions. The degree to which this happens is partially determined by CO_2 dissociation constants (k_1,k_2):

$$pCO_2 = \frac{k_2}{k_0 k_1} \frac{[HCO_3^-]^2}{[CO_3^{2-}]} \qquad eq.\ A2$$

We can approximate the concentration of carbonate ($[CO_3^{2-}]$) in terms of DIC and Alkalinity by subtracting the following two approximations of DIC and Alkalinity:

$$DIC \approx [HCO_3^-] + [CO_3^{2-}] \qquad eq.\ A3$$

$$Alk \approx [HCO_3^-] + 2[CO_3^{2-}] \qquad eq.\ A4$$

$$[CO_3^{2-}] \approx DIC - Alk \qquad eq.\ A5$$

Then substituting equation A5 into A4 we can similarly approximate bicarbonate ($[HCO_3^-]$):

$$[HCO_3^-] \approx 2DIC - Alk \qquad eq.\ A6$$

Substituting equation A5 and equation A6 into equation A2 yields:

$$pCO_2 \approx \frac{k_2}{k_0 k_1} \frac{(2DIC - Alk)^2}{(Alk - DIC)} \qquad eq.\ A7$$

If we reduce the initial salinity from 35 PSU to 32 PSU we can illustrate the effect of surface freshening on pCO_2. Given that meteoric water will add almost no alkalinity and negligible DIC, it only dilutes the concentration. To calculate the dilution we use the linearization from equation 3 in the main text, with no contribution to ΔDIC from the second term on the RHS. The solubility constants are affected by changes to salinity, but this effect is small. Using a contemporary surface ocean alkalinity concentration of 2340 μmol kg^{-1} and DIC concentration of 2090 μmol kg^{-1}, after dilution we arrive at a ΔpCO_2^{ocn} of -25 ppm. The approximation shows the dominance of DIC in this balance, DIC is contributing double to the balance in the numerator of the RHS of equation A7. While this equation illustrates the

dominance of DIC in driving the direction of the change, this approximation is not, however, suitable for quantifying the magnitude of the change because of the approximations of DIC and alkalinity used to derive equation A7.

References

Aagaard, K., and E. C. Carmack (1989), The role of sea ice and other fresh water in the Arctic circulation, Journal of Geophysical Research: Oceans, 94(C10), 14485-14498.

Alan, R. L. (2007), Ecological geography of the sea.

Barnhart, K. R., C. R. Miller, I. Overeem, and J. E. Kay (2016), Mapping the future expansion of Arctic open water, Nature Climate Change, 6(3), 280-285.

Carmack, E. C. (2000), The Arctic Ocean's Freshwater Budget: Sources, Storage and Export, in The Freshwater Budget of the Arctic Ocean, edited by E. L. Lewis, E. P. Jones, P. Lemke, T. D. Prowse and P. Wadhams, pp. 91-126, Springer Netherlands, Dordrecht.

Curry, B., C. M. Lee, B. Petrie, R. E. Moritz, and R. Kwok (2013), Multiyear Volume, Liquid Freshwater, and Sea Ice Transports through Davis Strait, 2004–10, Journal of Physical Oceanography, 44(4), 1244-1266.

Dai, A., and K. E. Trenberth (2002), Estimates of Freshwater Discharge from Continents: Latitudinal and Seasonal Variations, Journal of Hydrometeorology, 3(6), 660-687.

De Lavergne, C., J. B. Palter, E. D. Galbraith, R. Bernardello, and I. Marinov (2014), Cessation of deep convection in the open Southern Ocean under anthropogenic climate change, Nature Climate Change, 4(4), 278-282.

de Steur, L., E. Hansen, R. Gerdes, M. Karcher, E. Fahrbach, and J. Holfort (2009), Freshwater

fluxes in the East Greenland Current: A decade of observations, Geophysical Research Letters, 36(23).

DeVries, T. (2014), The oceanic anthropogenic CO2 sink: Storage, air-sea fluxes, and transports over the industrial era, Global Biogeochemical Cycles, 28(7), 631-647.

Dickson, R., B. Rudels, S. Dye, M. Karcher, J. Meincke, and I. Yashayaev (2007), Current estimates of freshwater flux through Arctic and subarctic seas, Progress in Oceanography, 73(3–4), 210-230.

Doney, S. C., I. Lima, R. A. Feely, D. M. Glover, K. Lindsay, N. Mahowald, J. K. Moore, and R. Wanninkhof (2009), Mechanisms governing interannual variability in upper-ocean inorganic carbon system and air–sea CO 2 fluxes: Physical climate and atmospheric dust, Deep Sea Research Part II: Topical Studies in Oceanography, 56(8), 640-655.

Fay, A. R., and G. A. McKinley (2014), Global open-ocean biomes: mean and temporal variability, Earth Syst. Sci. Data, 6(2), 273-284.

Gleick, P. H. (2000), The World's Water 2000 – 2001, edited, pp. 39-61, Island Press, Washington, D. C.

Gruber, N., et al. (2009), Oceanic sources, sinks, and transport of atmospheric CO2, Global Biogeochemical Cycles, 23(1).

Haine, T. W. N., et al. (2015), Arctic freshwater export: Status, mechanisms, and prospects, Global and Planetary Change, 125, 13-35.

Hattermann, T., P. E. Isachsen, W.-J. von Appen, J. Albretsen, and A. Sundfjord (2016), Eddy-driven recirculation of Atlantic Water in Fram Strait, Geophysical Research Letters, 43(7), 3406-3414.

Holland, M. M., J. Finnis, A. P. Barrett, and M. C. Serreze (2007), Projected changes in Arctic Ocean freshwater budgets, Journal of Geophysical Research: Biogeosciences, 112(G4).

Häkkinen, S., and P. B. Rhines (2004), Decline of Subpolar North Atlantic Circulation During the 1990s, Science, 304(5670), 555-559.

Jahn, A., B. Tremblay, L. A. Mysak, and R. Newton (2010), Effect of the large-scale atmospheric circulation on the variability of the Arctic Ocean freshwater export, Climate Dynamics, 34(2), 201-222.

Jahn, A., et al. (2011), Late-Twentieth-Century Simulation of Arctic Sea Ice and Ocean Properties in the CCSM4, Journal of Climate, 25(5), 1431-1452.

Jahn, A., et al. (2012), Arctic Ocean freshwater: How robust are model simulations?, Journal of Geophysical Research: Oceans, 117(C8).

Karcher, M., R. Gerdes, F. Kauker, C. Köberle, and I. Yashayaev (2005), Arctic Ocean change heralds North Atlantic freshening, Geophysical Research Letters, 32(21).

Kay, J. E., et al. (2014), The Community Earth System Model (CESM) Large Ensemble Project: A Community Resource for Studying Climate Change in the Presence of Internal Climate Variability, Bulletin of the American Meteorological Society, 96(8), 1333-1349.

Keeling, C. D., H. Brix, and N. Gruber (2004), Seasonal and long-term dynamics of the upper ocean carbon cycle at Station ALOHA near Hawaii, Global Biogeochemical Cycles, 18(4).

Khatiwala, S., F. Primeau, and T. Hall (2009), Reconstruction of the history of anthropogenic

CO2 concentrations in the ocean, Nature, 462(7271), 346-349.

Koenigk, T., L. Brodeau, R. G. Graversen, J. Karlsson, G. Svensson, M. Tjernström, U. Willén, and K. Wyser (2013), Arctic climate change in 21st century CMIP5 simulations with EC-Earth, Climate Dynamics, 40(11), 2719-2743.

Landschützer, P., N. Gruber, D. Bakker, and U. Schuster (2014), Recent variability of the global ocean carbon sink, Global Biogeochemical Cycles, 28(9), 927-949.

Marshall, J., and F. Schott (1999), Open-ocean convection: Observations, theory, and models, Reviews of Geophysics, 37(1), 1-64.

Morison, J., R. Kwok, C. Peralta-Ferriz, M. Alkire, I. Rigor, R. Andersen, and M. Steele (2012), Changing Arctic Ocean freshwater pathways, Nature, 481(7379), 66-70.

Polyakov, I. V., V. A. Alexeev, G. I. Belchansky, I. A. Dmitrenko, V. V. Ivanov, S. A. Kirillov, A. A. Korablev, M. Steele, L. A. Timokhov, and I. Yashayaev (2008), Arctic Ocean Freshwater Changes over the Past 100 Years and Their Causes, Journal of Climate, 21(2), 364-384.

Rawlins, M. A., et al. (2010), Analysis of the Arctic System for Freshwater Cycle Intensification: Observations and Expectations, Journal of Climate, 23(21), 5715-5737.

Rignot, E., I. Velicogna, M. R. van den Broeke, A. Monaghan, and J. T. M. Lenaerts (2011), Acceleration of the contribution of the Greenland and Antarctic ice sheets to sea level rise, Geophysical Research Letters, 38(5).

Rödenbeck, C., R. F. Keeling, D. C. E. Bakker, N. Metzl, A. Olsen, C. Sabine, and M. Heimann

(2013), Global surface-ocean p(CO2) and sea–air CO2 flux variability from an observation-driven ocean mixed-layer scheme, Ocean Sci., 9(2), 193-216.

Schuster, U., et al. (2013), An assessment of the Atlantic and Arctic sea–air CO2 fluxes, 1990–2009, Biogeosciences, 10(1), 607-627.

Serreze, M. C., and R. G. Barry (2011), Processes and impacts of Arctic amplification: A research synthesis, Global and Planetary Change, 77(1–2), 85-96.

Stouffer, R. J., et al. (2006), Investigating the Causes of the Response of the Thermohaline Circulation to Past and Future Climate Changes, Journal of Climate, 19(8), 1365-1387.

Swart, N. C., J. C. Fyfe, E. Hawkins, J. E. Kay, and A. Jahn (2015), Influence of internal variability on Arctic sea-ice trends, Nature Clim. Change, 5(2), 86-89.

Swingedouw, D., C. B. Rodehacke, S. M. Olsen, M. Menary, Y. Gao, U. Mikolajewicz, and J. Mignot (2015), On the reduced sensitivity of the Atlantic overturning to Greenland ice sheet melting in projections: a multi-model assessment, Climate Dynamics, 44(11), 3261-3279.

Takahashi, T., et al. (2009), Climatological mean and decadal change in surface ocean pCO2, and net sea–air CO2 flux over the global oceans, Deep Sea Research Part II: Topical Studies in Oceanography, 56(8–10), 554-577.

Thornalley, D. J. R., S. Barker, W. S. Broecker, H. Elderfield, and I. N. McCave (2011), The Deglacial Evolution of North Atlantic Deep Convection, Science, 331(6014), 202-205.

Vage, K., R. S. Pickart, V. Thierry, G. Reverdin, C. M. Lee, B. Petrie, T. A. Agnew, A. Wong, and

M. H. Ribergaard (2009), Surprising return of deep convection to the subpolar North Atlantic Ocean in winter 2007-2008, Nature Geosci, 2(1), 67-72.

Vavrus, S. J., M. M. Holland, A. Jahn, D. A. Bailey, and B. A. Blazey (2011), Twenty-First-Century Arctic Climate Change in CCSM4, Journal of Climate, 25(8), 2696-2710.

Yamamoto-Kawai, M., F. A. McLaughlin, E. C. Carmack, S. Nishino, K. Shimada, and N. Kurita (2009), Surface freshening of the Canada Basin, 2003–2007: River runoff versus sea ice meltwater, Journal of Geophysical Research: Oceans, 114(C1).